photonics

MDPI

Article

Secrecy Rate Bounds in Spatial Modulation-Based Visible Light Communications under Signal-Dependent Noise Conditions

Yahya M. Al-Moliki [1,*], Ali H. Alqahtani [1], Mohammed T. Alresheedi [2] and Yahya Al-Harthi [2]

[1] Department of Applied Electrical Engineering, Al-Muzahimya Campus, College of Applied Engineering, King Saud University, P.O. Box 2454, Riyadh 11421, Saudi Arabia; ahqahtani@ksu.edu.sa
[2] Department of Electrical Engineering, College of Engineering, King Saud University, P.O. Box 800, Riyadh 11421, Saudi Arabia; malresheedi@ksu.edu.sa (M.T.A.); yalharthi@ksu.edu.sa (Y.A.-H.)
* Correspondence: yalmoliki@ksu.edu.sa

Abstract: This study examines the physical-layer security of an indoor visible light communication (VLC) system using spatial modulation (SM), which consists of several transmitters, an authorized receiver, and a passive adversary. The SM technique is applied at the transmitters so that only one transmitter is operational at any given time. A uniform selection (US) strategy is employed to choose the active transmitter. The two scenarios under examination encompass the conditions of non-negativity and average optical intensity, as well as the conditions of non-negativity, average optical intensity, and peak optical intensity. The secrecy rate is then obtained for these two scenarios while accounting for both signal-independent noise and signal-dependent noise. Additionally, the high signal-to-noise ratio (SNR) asymptotic behavior of the derived secrecy rate constraints is investigated. A channel-adaptive selection (CAS) strategy and a greedy selection (GS) scheme are utilized to select the active transmitter, aiming to enhance the secrecy performance. The current numerical findings affirm a pronounced convergence between the lower and upper bounds characterizing the secrecy rate. Notably, marginal asymptotic differentials in performance emerge at elevated SNRs. Furthermore, the GS system outperforms the CAS scheme and the US method, in that order. Additionally, the impact of friendly optical jamming on the secrecy rate is investigated. The results show that optical jamming significantly enhances the secrecy rate, particularly at higher power levels.

Keywords: physical-layer security; secrecy rate; spatial modulation; signal-independent noise; signal-dependent noise; visible light communications

Citation: Al-Moliki, Y.M.; Alqahtani, A.H.; Alresheedi, M.T.; Al-Harthi, Y. Secrecy Rate Bounds in Spatial Modulation-Based Visible Light Communications under Signal-Dependent Noise Conditions. *Photonics* **2024**, *11*, 934. https://doi.org/10.3390/photonics11100934

Received: 12 August 2024
Revised: 23 September 2024
Accepted: 30 September 2024
Published: 3 October 2024

1. Introduction

Multi-input multi-output (MIMO) is one of the most promising strategies for wireless communication networks, including vehicular ad hoc networks and fifth-/sixth-generation (5G/6G) networks [1]. However, MIMO schemes typically involve high hardware complexity due to the need for multiple radio frequency (RF) chains. To address this limitation, a low-complexity alternative called spatial modulation (SM), which uses a single RF chain, was developed [2,3]. In SM, only one antenna is activated in each time slot, while the others remain inactive. The index of the active antenna is encoded into a portion of the input bits at the transmitter. As a result, the signal's dimensionality increases, enhancing the transmission rate. Both the transmitted signal and the active antenna index are recovered at the receiver. Readers can refer to [4] for more detailed information on SM.

SM has gained increasing attention for its ability to balance spectral efficiency and energy efficiency, while maintaining a simple design through the use of a single RF chain. A comprehensive survey of recent developments in SM, including its applications across various domains such as time, frequency, and code, as well as its integration with emerging wireless technologies, is provided in [5]. Furthermore, the potential of SM in 6G networks is highlighted in [6], where the concept of index modulation multiple access is explored

to enhance system performance and enable massive connectivity, further extending the applicability of SM in future communication systems.

Conventional wireless communication systems, such as RF-based systems, operate in a spectrum that is highly susceptible to interference, fading, and congestion due to the shared nature of radio frequency bands. In contrast, Visible Light Communication (VLC) operates in a much larger, unregulated spectrum (400–800 THz), offering several advantages over traditional RF channels. VLC signals, transmitted through optical light, provide higher directivity and have a limited propagation range, reducing interference risk and enhancing spatial security. Moreover, VLC is highly resistant to electromagnetic interference, which is common in RF systems. However, due to its broadcast nature and line-of-sight requirements, VLC channels are also vulnerable to eavesdropping attacks. This makes physical-layer security techniques especially critical for VLC systems. These differences between VLC and conventional wireless channels necessitate specialized approaches to ensure data confidentiality, as explored in this study.

Significant reports on SM have demonstrated its advantages over MIMO. Recently, increasing attention has been directed toward research on SM in VLC systems [2,7]. VLC is a promising wireless technology that complements traditional RF systems due to its use of the open and unregulated light spectrum (400–800 THz). Optical signals offer higher directivity and greater resistance to obstacles compared to RF, enhancing security. However, VLC communications are vulnerable to eavesdropping due to the broadcast nature of the optical link. The topic of security in VLC has been studied in [8,9], where physical-layer security methods were identified as innovative and effective strategies for improving data confidentiality [10].

In [11–14], the authors analyzed physical-layer security in single-input-single-output (SISO) VLC systems, deriving tight upper and lower bounds on secrecy capacity under average and peak optical intensity constraints. In [15–19], various aspects of physical-layer security in multi-user VLC systems were addressed, including secrecy sum rates, performance in 3D networks, secrecy outage probabilities, and novel spatial constellation designs aimed at enhancing security and reducing eavesdropping. In [20–25], the focus shifted to multiple-input-single-output (MISO) VLC systems, where the authors explored secure beamforming under various channel state information (CSI) conditions, addressing amplitude constraints, non-line-of-sight effects, and inter-symbol interference to optimize secrecy rates. Lastly, in [26–31], techniques like jamming and AN-aided precoding were employed to maximize secrecy rates, while in [32,33], both secure beamforming and artificial noise (AN) jamming were combined for further secrecy rate enhancement.

Secret-key secrecy methods [34–38] have been developed to derive secret keys from physical-layer signals, such as orthogonal frequency division multiplexing signals, to enhance the security of VLC systems. The studies referenced in [11–38] analyzed secrecy performance under the assumption of signal-independent interfering noise, which is an unrealistic assumption for VLC systems. In contrast, [39] and [40] investigated the secrecy performance of SISO VLC systems with the more realistic assumption that the interfering noise depends on the signal.

While numerous studies have investigated methods to enhance the confidentiality of VLC in SISO- and MISO/MIMO-based spatial multiplexing systems [11–40], there is a limited body of literature specifically addressing the secrecy rate in VLC-based SM systems [41–45].

For the studies related to VLC-based SM systems [41–45], upper and lower bounds on VLC secrecy rates were derived under the assumption of signal-independent noise, which is impractical for VLC systems. In contrast, this study investigates the secrecy rate within a three-indoor SM-based VLC scheme, accounting for signal-dependent noise. We also propose random noise variances for both the intended user and the adversary. The key contributions of this work are as follows:

- We assess the secrecy rate for SM-based VLC under non-negativity and average optical intensity constraints. We derive a lower bound using the uniform selection (US)

mechanism and an upper bound using the dual expression of the secrecy rate, with closed-form expressions for both bounds. Numerical results confirm the reliability of these bounds.
- We analyze SM-based VLC with constraints on non-negativity, average optical intensity, and peak optical intensity. Closed-form expressions for the secrecy rate bounds, including the peak optical intensity constraint, are derived. Numerical results demonstrate that the bounds are tightly constrained.
- We evaluate the asymptotic performance of the secrecy rate at high optical intensity. The difference between the lower and upper bounds is minimal at high signal-to-noise ratios (SNR).
- To enhance secrecy performance, we employ the channel-adaptive selection (CAS) method and the greedy selection (GS) method for active transmitter selection. The GS method outperforms both the CAS and US methods, as demonstrated by numerical results.
- We investigate the impact of friendly optical jamming on the secrecy rate. The results show that optical jamming significantly improves the secrecy rate, particularly at higher power levels.

The remainder of this work is structured as follows: Section 2 introduces the system model. Sections 3 and 4 analyze two scenarios, presenting the secrecy rate bounds and asymptotic performance for SM-based VLC. Section 5 discusses two transmitter selection strategies to enhance secrecy performance. Section 6 proposes an optical jamming technique for further improving secrecy. Section 7 examines a scenario with multiple receivers. Section 8 presents the numerical results. Section 9 provides the discussion, and Section 10 concludes the work.

2. System Model

Figure 1 depicts an indoor VLC system with M emitters, representing Alice (the transmitter), an authorized receiver (Bob), and an adversary (Eve). Each emitter, positioned on the roof, uses a light emitting diode (LED) to transmit optical signals. SM is employed by Alice, meaning that only one LED is activated at a time while the others remain inactive. Figure 2 illustrates the SM schematic in VLC. Both Bob and Eve are situated on the ground, each equipped with a photodiode (PD) for converting optical signals to electrical signals. When an active LED transmits data to Bob, Eve may also intercept the message.

The primary sources of noise at the receivers of Alice and Bob include both signal-independent and signal-dependent noise [11]. At any given time, the m-th LED is activated. Consequently, the signals received by Bob and Eve are described as follows:

$$\begin{cases} Y_B = h_{B,m}X + \sqrt{h_{B,m}X}Z_{B,1} + Z_{B,0} \\ Y_E = h_{E,m}X + \sqrt{h_{E,m}X}Z_{E,1} + Z_{E,0} \end{cases}, \; m = 1, 2, \ldots, M, \tag{1}$$

where $Z_{B,0} \sim \mathcal{N}(0, \sigma_B^2)$ and $Z_{E,0} \sim \mathcal{N}(0, \sigma_E^2)$ denote the signal-independent noise at Bob and Eve, with σ_B^2 and σ_E^2 representing the noise variances. Similarly, $Z_{B,1} \sim \mathcal{N}(0, \varsigma_B^2\sigma_B^2)$ and $Z_{E,1} \sim \mathcal{N}(0, \varsigma_E^2\sigma_E^2)$ denote the signal-dependent noise at Bob and Eve, where ς_B^2 and ς_E^2 (with ς_B^2, $\varsigma_E^2 > 0$) are the ratios of signal-dependent noise variance to signal-independent noise variance. $h_{B,m}$ and $h_{E,m}$ are the instantaneous channel gains from the m-th LED to the receivers at Bob and Eve, respectively, as specified in Equation (6) of [35].

SM activates only one LED at a time, using the US mechanism, where each LED has an equal probability of being selected. Consequently, the probability $p(h_k = h_{k,m})$ is written as

$$p(h_k = h_{k,m}) = \frac{1}{M}, \; k = B \text{ or } E \tag{2}$$

We consider the following signal constraints for indoor VLC [11]:

- *Nonnegativity:* The input signal X in (1) is a nonnegative random variable representing the optical signal's intensity. Consequently, we have

$$X \geq 0. \tag{3}$$

- *Peak optical intensity constraint:* The input signal is typically subject to a peak optical intensity constraint, imposed by practical and safety limitations.

$$X \leq A, \tag{4}$$

- *Average optical intensity constraint:* Since VLC requires constant illumination, the average optical intensity must remain stable over time but can be adjusted to meet user needs. Thus, the average optical intensity constraint is described as

$$E_x(X) = \xi P, \tag{5}$$

where $\xi \in (0, 1]$ and P denote the dimming target and the nominal optical intensity of the LED, respectively.

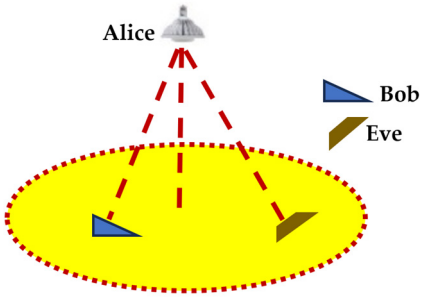

Figure 1. System model.

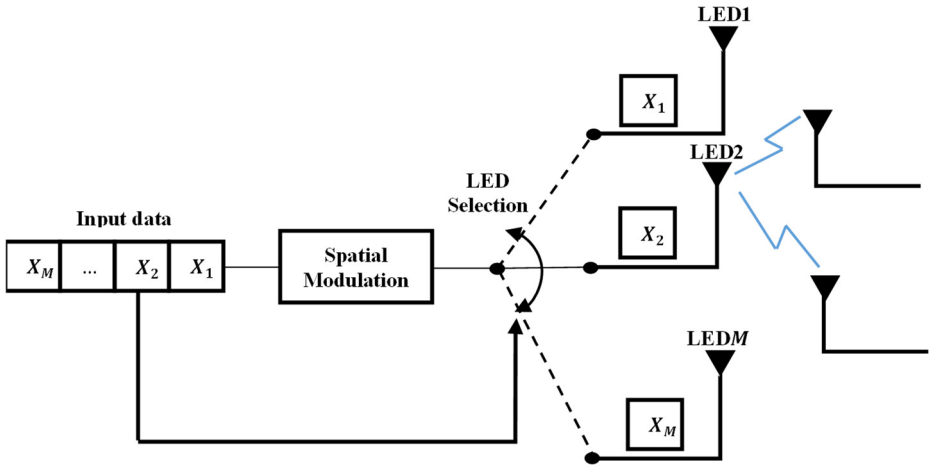

Figure 2. The SM schematic in VLC.

3. Secrecy Rate for SM-Based VLC with Constraints (3) and (5)

This section analyzes the secrecy rate bounds for SM-based VLC under constraints (3) and (5). Additionally, it provides the secrecy rate asymptotic at large SNR. According to information theory [21], no secrecy rate is achievable if the main channel is worse than

the adversary's channel. Conversely, a positive secrecy rate R_s for SM-based VLC with constraints (3) and (5) can be computed by solving the following problem:

$$\begin{aligned} R_s = \max_{f_X(x)} & [I(X, h_B; Y_B) - I(X, h_E; Y_E)] \\ \text{s.t. } & \textstyle\int_0^\infty f_X(x)\mathrm{d}x = 1, \\ & \mathbb{E}(X) = \textstyle\int_0^\infty x f_X(x)\mathrm{d}x = \xi P, \end{aligned} \tag{6}$$

where $f_X(x)$ represents the probability density function (PDF) of X, and $I(;)$ denotes the mutual information. Note that solving the optimization problem (6) is highly challenging. We will, however, closely examine constrained secrecy rate bounds in the following section.

3.1. Lower Bound of Secrecy Rate

An arbitrary input PDF $f_X(x)$ that satisfies constraints (3) and (5) can be used to derive a lower bound on the secrecy rate in optimization problem (6) as follows:

$$\begin{aligned} R_s &= \max_{f_X(x)} \tfrac{1}{M} \textstyle\sum_{m=1}^{M} \Big[I(X, h_{B,m}; Y_B) - \sum_{m=1}^{M} I(X, h_{E,m}; Y_E) \Big] \\ &= \max_{f_X(x)} \tfrac{1}{M} \textstyle\sum_{m=1}^{M} [\mathcal{H}(Y_B) - \mathcal{H}(Y_E) + \mathcal{H}(Y_E|h_{E,m}, X) - \mathcal{H}(Y_B|h_{B,m}, X)], \end{aligned} \tag{7}$$

where $\mathcal{H}(\cdot)$ represents the entropy. In accordance with (1), the PDF of $f_{Y_k|h_{k,m}}(y_k|h_{k,m}, x)$, $k = B$ or E, can be obtained as

$$f_{Y_k|h_{k,m}}(y_k|h_{k,m}, x) = \frac{e^{\left[-\frac{(y_k - h_{k,m}x)^2}{2(1+h_{k,m}X\varsigma_k^2)\sigma_k^2}\right]}}{\sqrt{2\pi(1 + h_{k,m}X\varsigma_k^2)\sigma_k^2}}. \tag{8}$$

Thus, $\mathcal{H}(Y_k|h_{k,m}, X)$ is computed as

$$\mathcal{H}(Y_k|h_{k,m}, X) = \frac{1}{2}\ln\left(2\pi e\sigma_k^2\right) + \frac{1}{2}\mathbb{E}_x\left[\ln\left(1 + h_{k,m}X\varsigma_k^2\right)\right]. \tag{9}$$

Moreover, $\mathcal{H}(Y_E)$ is constrained by the upper limit determined by the differential entropy of a Gaussian random variable with variance of $\mathrm{var}(Y_E)$ [46], as follows:

$$\mathcal{H}(Y_E) \le \frac{1}{2}\ln[2\pi e\mathrm{var}(Y_E)]. \tag{10}$$

As stated in proposition 11 of [47], The output entropy exceeding the input entropy implies that $\mathcal{H}$ can be lower-bounded by

$$\mathcal{H}(Y_B) \ge \mathcal{H}(X) + f_{low}(h_{B,m}, \xi, P), \tag{11}$$

where $f_{low}(h_{B,m}, \xi, P)$ is computed as follows:

$$f_{low}(h_{B,m}, \xi, P) = \frac{1}{2}\ln\left(h_{B,m}^2 + \frac{2h_{B,m}\varsigma_B^2\sigma_B^2}{\xi P}\right) - \frac{h_{B,m}\xi P + \varsigma_B^2\sigma_B^2}{\varsigma_B^2\sigma_B^2} + \frac{\sqrt{h_{B,m}\xi P\left(h_{B,m}\xi P + 2\varsigma_B^2\sigma_B^2\right)}}{\varsigma_B^2\sigma_B^2}. \tag{12}$$

We can rewrite the lower bound by substituting (9)–(11) into (7) as

$$R_s \ge \frac{1}{M}\sum_{m=1}^{M}\left(f_{low}(h_{B,m}, \xi, P) + \frac{1}{2}\mathbb{E}_x\left[\ln\left(\frac{1 + h_{E,m}X\varsigma_E^2}{1 + h_{B,m}X\varsigma_B^2}\right)\right]\right) + \mathcal{H}(X) - \frac{1}{2}\ln[2\pi e\mathrm{var}(Y_E)] + \frac{1}{2}\ln\left(\frac{\sigma_E^2}{\sigma_B^2}\right). \tag{13}$$

As shown in (13), we obtain a lower bound on the secrecy rate by choosing a PDF that satisfies the constraints of problem (6). To achieve a tight lower bound, we select an

appropriate input PDF. Using the variational method, we derive this lower bound on the secrecy rate.

Theorem 1. *The lower bound for the secrecy rate in SM-based VLC with constraints (3) and (5) is given by*

$$R_s \geq \frac{1}{M}\sum_{m=1}^{M}\left(\frac{1}{2}ln\left[\frac{e\xi^2P^2\sigma_E^2}{2\pi\sigma_B^2\left(h_{E,m}^2\xi^2P^2+h_{E,m}\xi P\varsigma_E^2\sigma_E^2+\sigma_E^2\right)}\right]+f_{low}(h_{B,m},\xi,P)+\frac{1}{2}\left[e^{\frac{1}{h_{B,m}\varsigma_B^2\xi P}}\mathbb{E}i\left(-\frac{1}{h_{B,m}\varsigma_B^2\xi P}\right)-e^{\frac{1}{h_{E,m}\varsigma_E^2\xi P}}\mathbb{E}i\left(-\frac{1}{h_{E,m}\varsigma_E^2\xi P}\right)\right]\right). \quad (14)$$

When $M = 1$ (SISO system), the secrecy rate bound in (19) coincides with (14) in [40].

Proof. See Appendix A. □

Corollary 1. *In the scenario of assuming signal-independent noise (i.e., ς_E^2, $\varsigma_B^2 \to 0$), the secrecy rate lower bound given in (14) simplifies to (15), which coincides with (7) in* [44].

$$R_s \geq \frac{1}{2M}\sum_{m=1}^{M} ln\left[\frac{e\xi^2P^2\sigma_E^2}{2\pi\sigma_B^2\left(h_{E,m}^2\xi^2P^2+\sigma_E^2\right)}\right], \quad (15)$$

3.2. Upper Bound of Secrecy Rate

In this section, we use the dual expression of the secrecy rate [44] to analyze the upper bound. To simplify the derivation, we rewrite (1) as

$$\begin{cases}\grave{Y}_{B,m} = X+\sqrt{h_{B,m}X}\grave{Z}_{B,1,m}+\grave{Z}_{B,0,m}\\ \grave{Y}_{E,m} = X+\sqrt{h_{E,m}X}\grave{Z}_{E,1,m}+\grave{Z}_{E,0,m}\end{cases}, \quad (16)$$

where $\grave{Y}_{B,m} = Y_B/h_{B,m}$, $\grave{Y}_{E,m} = Y_E/h_{E,m}$, $\grave{Z}_{B,1,m} = Z_{B,1}/h_{B,m}$, $\grave{Z}_{E,1,m} = Z_{E,1}/h_{E,m}$, $\grave{Z}_{B,0,m} = Z_{B,0}/h_{B,m}$, and $\grave{Z}_{E,0,m} = Z_{E,0}/h_{E,m}$.

The following inequality is valid for any random conditional PDF $g_{\grave{Y}_{B,m}|\grave{Y}_{E,m}}\left(\hat{y}_{B,m}\middle|\grave{Y}_{E,m}\right)$:

$$I\left(X;\grave{Y}_{B,m}\middle|\grave{Y}_{E,m}\right) \leq \mathbb{E}_{X\grave{Y}_{E,m}}\{u\}, \quad (17)$$

where u indicates to a relative entropy, stated as

$$u = D\left(f_{\grave{Y}_{B,m}|X\grave{Y}_{E,m}}\left(\hat{y}_{B,m}\middle|X,\grave{Y}_{E,m}\right)\middle\|g_{\grave{Y}_{B,m}|\grave{Y}_{E,m}}\left(\hat{y}_{B,m}\middle|\grave{Y}_{E,m}\right)\right). \quad (18)$$

To obtain an upper bound,

$$I\left(X;\grave{Y}_{B,m}\middle|\grave{Y}_{E,m}\right) = \min_{g_{\grave{Y}_{B,m}|\grave{Y}_{E,m}}(\hat{y}_{B,m}|\grave{Y}_{E,m})}\mathbb{E}_{X\grave{Y}_{E,m}}\{u\}. \quad (19)$$

Following (6), R_s can be re-written as

$$R_s = \max_{f_X(x)}\frac{1}{M}\sum_{m=1}^{M} I\left(X;\grave{Y}_{B,m}\middle|\grave{Y}_{E,m}\right). \quad (20)$$

An optimal solution for $\frac{1}{M}\sum_{m=1}^{M} I\left(X;\grave{Y}_{B,m}\middle|\grave{Y}_{E,m}\right)$ can be achieved by using a specific input PDF $f_X(x)$ while satisfying constraints (3) and (5). The secrecy rate R_s in (20) is re-expressed as

$$R_s = \frac{1}{M}\sum_{m=1}^{M}\left\{\min_{g_{\grave{Y}_{B,m}|\grave{Y}_{E,m}}(\hat{y}_{B,m}|\grave{Y}_{E,m})}\mathbb{E}_{X^*\grave{Y}_{E,m}}\{u\}\right\}, \quad (21)$$

where X^* and $f_{X^*}(x)$ denote the optimal input and its associated PDF. To establish a tight upper bound on the secrecy rate, we need to select a tractable and appropriate $g_{\dot{Y}_{B,m}|\dot{Y}_{E,m}}\left(\dot{y}_{B,m}\middle|\dot{Y}_{E,m}\right)$. Consequently, the following problem arises:

Theorem 2. *In the context of SM-based VLC having constraints (3) and (5), the secrecy rate is upper-bounded by*

$$R_s \leq \begin{cases} \frac{1}{M}\sum_{m=1}^{M} ln\left(\sqrt{\frac{4eh_{E,m}\varsigma_E^2\sigma_E^2}{\pi^2 M}}+\sqrt{\frac{2e\xi P h_{B,m}h_{E,m}\varsigma_E^2\sigma_E^2}{\pi M\varsigma_B^2\sigma_B^2}}\right), \\ \quad if\ \frac{1}{\sqrt{2\pi}} \geq \frac{h_{E,m}}{h_{B,m}}\left(\sqrt{\frac{h_{B,m}\varsigma_B^2\sigma_B^2}{2\pi M}}+\frac{h_{B,m}}{2}\sqrt{\frac{\xi P}{M}}\right) \\ \frac{1}{2M}\sum_{m=1}^{M} ln\left(\frac{4eh_{B,m}\varsigma_E^2\sigma_E^2}{\pi^2 h_{E,m}\varsigma_B^2\sigma_B^2}\right),\ otherwise \end{cases} \tag{22}$$

where $M = h_{E,m}^2\varsigma_B^2\sigma_B^2/h_{B,m} + h_{E,m}\varsigma_E^2\sigma_E^2$.

When $M = 1$ (SISO system), the secrecy rate bound in (22) coincides with (21) in [40].

Proof. See Appendix B. □

Corollary 2. *Assuming signal-dependent noise is disregarded in Theorem 2, secrecy rate upper bound (22) simplifies to (23), which coincides with (15) in* [44].

$$\lim_{\substack{\varsigma_B\to 0\\ \varsigma_E\to 0}} R_s \leq \begin{cases} \frac{1}{M}\sum_{m=1}^{M} ln\left[\frac{4e\left(\frac{\sigma_B}{\sqrt{2\pi}}+\frac{h_{B,m}\xi P}{2}\right)}{\sqrt{2\pi e\sigma_B^2\left(1+\frac{\sigma_B^2 h_{E,m}^2}{\sigma_E^2 h_{B,m}^2}\right)}}\right], \\ if\ \frac{1}{\sqrt{2\pi}} \geq \frac{h_{E,m}}{\sqrt{\sigma_B^2 h_{E,m}^2+\sigma_E^2 h_{B,m}^2}}\left(\frac{\sigma_B}{\sqrt{2\pi}}+\frac{h_{B,m}\xi P}{2}\right) \\ \frac{1}{M}\sum_{m=1}^{M} ln\left(\frac{2\sqrt{e}h_{B,m}\sigma_E}{\pi h_{E,m}\sigma_B}\right),\ otherwise \end{cases} \tag{23}$$

3.3. Asymptotic Behavior Analysis

Indoor VLC typically operates with a high SNR, often exceeding 30 dB. Therefore, we focus on analyzing secrecy in high SNR conditions.

Corollary 3. *Exploring the upper and lower bounds of secrecy rates under constraints (3) and (5) as P approaches infinity as*

$$\begin{aligned} \lim_{P\to\infty} R_s &\geq \tfrac{1}{2}\ln\left(\tfrac{e}{2\pi}\right)+\tfrac{1}{2M}\sum_{m=1}^{M}\ln\left(\frac{h_{B,m}\varsigma_E^2\sigma_E^2}{h_{E,m}\varsigma_B^2\sigma_B^2}\right) \\ \lim_{P\to\infty} R_s &\leq \tfrac{1}{2}ln\left(\tfrac{4e}{\pi^2}\right)+\tfrac{1}{2M}\sum_{m=1}^{M} ln\left(\frac{h_{B,m}\varsigma_E^2\sigma_E^2}{h_{E,m}\varsigma_B^2\sigma_B^2}\right). \end{aligned} \tag{24}$$

Proof. See Appendix C. □

Remark 1. *Lower and higher asymptotic secrecy rate bounds differ by* $\frac{1}{2}ln\left(\frac{4e}{\pi^2}\right)-\frac{1}{2}ln\left(\frac{e}{2\pi}\right)\approx 0.4674$ *nat/transmission. Asymptotically, the performance gap is insignificant.*

4. Secrecy Rate for SM-Based VLC with Constraints (3)–(5)

By introducing an additional peak optical intensity constraint on the channel input, we derive more accurate and asymptotic secrecy rate bounds for the SM-based VLC

system. The computation of the secrecy rate involves addressing the following optimization problem while considering constraints (3)–(5):

$$\begin{aligned} R_s &= \max_{f_X(x)} [I(X, h_B; Y_B) - I(X, h_E; Y_E)] \\ &\quad : \text{s.t. } \int_0^A f_X(x)\mathrm{d}x = 1 \\ &\mathbb{E}(X) = \int_0^A x f_X(x)\mathrm{d}x = \xi P, \end{aligned} \tag{25}$$

Similar to (6), deriving the exact secrecy rate formulation for problem (25) is challenging. In the next two sections, we will derive both upper and lower bounds on the secrecy rate.

4.1. Lower Bound of Secrecy Rate

A lower bound on the secrecy rate for problem (25) can be obtained by selecting an arbitrary input PDF that satisfies criteria (3)–(5), as follows:

$$\begin{aligned} R_s &\geq \tfrac{1}{M} \textstyle\sum_{m=1}^{M} \Big[I(X, h_{B,m}; Y_B) - \sum_{m=1}^{M} I(X, h_{E,m}; Y_E) \Big] \\ &= \tfrac{1}{M} \textstyle\sum_{m=1}^{M} [\mathcal{H}(Y_B) - \mathcal{H}(Y_B|h_{B,m}, X) - \mathcal{H}(Y_E) + \mathcal{H}(Y_E|h_{E,m}, X)], \end{aligned} \tag{26}$$

In this instance, the lower bound on the secrecy rate (13) is applicable. Define the ratio of the average optical intensity to the peak optical intensity as $\alpha = \xi P / A$. The following theorem establishes a lower bound for this ratio.

Theorem 3. *Our lower bound on the secrecy rate for SM-based VLC, subject to constraints (3)–(5) is as follows:*

$$R_s \geq \begin{cases} R_{s1}, \ if \ \alpha = 0.5 \\ R_{s2}, \ if \ \alpha \neq 0.5, \end{cases} \tag{27}$$

where R_{s1} and R_{s2} are expressed as

$$\begin{aligned} R_{s1} = \tfrac{1}{M} \textstyle\sum_{m=1}^{M} \Bigg(& f_{low}(h_{B,m}, \xi, P) + \tfrac{1}{2} \ln \left[\frac{6A^2\sigma_E^2}{\pi e \sigma_B^2 \left(h_{E,m}^2 A^2 + 6A h_{E,m} \varsigma_E^2 \sigma_E^2 + 12\sigma_E^2 \right)} \right] + \tfrac{1}{2} \ln \left(\frac{1 + h_{E,m} A \varsigma_E^2}{1 + h_{B,m} A \varsigma_B^2} \right) - \frac{\ln\left(1 + h_{B,m} A \varsigma_B^2\right)}{2A h_{B,m} \varsigma_B^2} + \\ & \frac{\ln\left(1 + h_{E,m} A \varsigma_E^2\right)}{2A h_{E,m} \varsigma_E^2} \Bigg), \end{aligned} \tag{28}$$

$$\begin{aligned} R_{s2} = \tfrac{1}{M} \textstyle\sum_{m=1}^{M} \Bigg(& f_{low}(h_{B,m}, \xi, P) + \tfrac{1}{2(e^{cA}-1)} \Bigg\{ \ln\left(\tfrac{1 + h_{E,m} A \varsigma_E^2}{1 + h_{B,m} A \varsigma_B^2} \right) e^{cA} - e^{-\frac{c}{h_{E,m}\varsigma_E^2}} \left[Ei\left(\tfrac{c}{h_{E,m}\varsigma_E^2} \left(1 + h_{E,m} A \varsigma_E^2 \right) \right) - Ei\left(\tfrac{c}{h_{E,m}\varsigma_E^2} \right) \right] + \\ & e^{-\frac{c}{h_{B,m}\varsigma_B^2}} \left[Ei\left(\tfrac{c}{h_{B,m}\varsigma_B^2} \left(1 + h_{B,m} A \varsigma_B^2 \right) \right) - Ei\left(\tfrac{c}{h_{B,m}\varsigma_B^2} \right) \right] \Bigg\} - \tfrac{1}{2} \ln \Big[2\pi e \Big(h_{E,m}^2 \left(\tfrac{A(cA-2)}{c(1-e^{-cA})} + \tfrac{2}{c^2} - \xi^2 P^2 \right) + h_{E,m} \xi P \varsigma_E^2 \sigma_E^2 + \sigma_E^2 \Big) \Big] \Bigg) - \\ & c\xi P + \tfrac{1}{2} \ln \left(\tfrac{\sigma_E^2}{\sigma_B^2} \tfrac{\left(e^{cA}-1\right)^2}{c^2} \right) \end{aligned} \tag{29}$$

where c in (29) can be computed from the following equation:

$$\alpha = \frac{1}{1 - e^{-cA}} - \frac{1}{cA} \tag{30}$$

When $M = 1$ (SISO system), the secrecy rate bounds in (28) and (29) coincide with (27) and (28) in [40].

Proof. See Appendix D. □

Corollary 4. *When signal-dependent noise is ignored, the secrecy rate lower bound (27) becomes*

$$\lim_{\substack{\varsigma_B\to 0\\ \varsigma_E\to 0}} R_s \begin{cases} \frac{1}{2M}\sum_{m=1}^{M} ln\left[\frac{3h_{B,m}^2\sigma_E^2A^2}{2\pi e\sigma_B^2\left(\xi^2P^2h_{E,m}^2+3\sigma_E^2\right)}\right] \; if\ \alpha = 0.5 \\ \frac{1}{2M}\sum_{m=1}^{M} ln\left[\frac{h_{B,m}^2\sigma_E^2e^{-2c\xi P}\left(\frac{e^{cA}-1}{c}\right)^2}{2\pi e\sigma_B^2\left(\frac{h_{E,m}^2A(cA-2)}{c\left(1-e^{-cA}\right)}+\frac{2h_{E,m}^2}{c^2}-h_{E,m}^2\xi^2P^2+\sigma_E^2\right)}\right],\ If\ \alpha \neq 0.5 \end{cases} \tag{31}$$

4.2. Upper Bound of Secrecy Rate

The dual expression in (20) for the secrecy rate remains valid even with the additional peak optical intensity constraint. The following theorem is derived from (21) and *Theorem 2*.

Theorem 4. *We obtain an upper bound for the secrecy rate in SM-based VLC, considering constraints (3)–(5) as follows:*

$$R_s \le \frac{1}{2M}\sum_{m=1}^{M} \ln\left[\frac{h_{E,m}\varsigma_E^2\sigma_E^2\left(h_{B,m}A+\varsigma_B^2\sigma_B^2\right)}{\varsigma_B^2\sigma_B^2\left(h_{E,m}^2A+\frac{h_{E,m}^2}{h_{B,m}}\varsigma_B^2\sigma_B^2+M\right)}\right], \tag{32}$$

where $M = h_{E,m}^2\varsigma_B^2\sigma_B^2/h_{B,m} + h_{E,m}\varsigma_E^2\sigma_E^2$.

When $M = 1$ (SISO system), the secrecy rate bounds in (32) coincide with (31) in [40].

Proof. See Appendix E. □

Corollary 5. *In Theorem 4, ignoring signal-dependent noise reduces the secrecy rate upper bound to*

$$\lim_{\substack{\varsigma_B\to 0\\ \varsigma_E\to 0}} R_s \le \frac{1}{2M}\sum_{m=1}^{M} ln\left[\frac{\left(h_{B,m}^2A\xi P+\sigma_B^2\right)\sigma_E^2}{\left(h_{E,m}^2A\xi P+2\frac{h_{E,m}^2}{h_{B,m}^2}\sigma_B^2+\sigma_E^2\right)\sigma_B^2}\right]. \tag{33}$$

Remark 2. *When signal-dependent noise is not taken into account, the upper bound on the secrecy rate for SM-based VLC in (33) coincides with (22) in* [44]. *This shows that the results in* [44] *are merely a specific instance of this paper's Theorem 4.*

4.3. Asymptotic Behavior Analysis

As the peak optical intensity of LED A approaches infinity, the asymptotic secrecy rate bounds can be obtained, as stated in *Theorems 3* and *4*.

Corollary 6. *We obtain asymptotic lower and upper bounds on secrecy rate for SM-based VLC satisfying constraints (3)–(5) as*

$$\begin{cases} \lim\limits_{A\to\infty} R_s \ge \begin{cases} \frac{1}{2M}\sum_{m=1}^{M} ln\left(\frac{6h_{B,m}\varsigma_E^2\sigma_E^2}{\pi eh_{E,m}\varsigma_B^2\sigma_B^2}\right),\ \ if\ \alpha = 0.5 \\ \frac{1}{2M}\sum_{m=1}^{M} ln\left[\frac{h_{B,m}h_{E,m}\varsigma_E^2\sigma_E^2\left(e^{cA}-1\right)^2}{2\pi ec^2\varsigma_B^2\sigma_B^2e^{2c\xi P}\left[h_{E,m}^2\left(\frac{A(cA-2)}{c\left(1-e^{-cA}\right)}+\frac{2}{c^2}-\xi^2P^2\right)+h_{E,m}\xi P\varsigma_E^2\sigma_E^2+\sigma_E^2\right]}\right],\ if\ \alpha \neq 0.5 \end{cases} \\ \lim\limits_{A\to\infty} R_s \le \frac{1}{2M}\sum_{m=1}^{M} ln\left(\frac{h_{B,m}\varsigma_E^2\sigma_E^2}{h_{E,m}\varsigma_B^2\sigma_B^2}\right). \end{cases} \tag{34}$$

Proof. See Appendix F. □

Remark 3. *In Corollary 6, when* $\alpha = 0.5$, *the difference between the asymptotic upper bound and the asymptotic lower bound is* $\frac{1}{2}ln\left(\frac{\pi e}{6}\right) \approx 0.1765$ *Nat/transmission. This means that the asymptotic performance difference is insignificant.*

When $\alpha \neq 0.5$, obtaining an exact asymptotic lower bound on the secrecy rate is challenging. Thus, the evaluation of the performance gap between the upper and lower bounds relies on numerical results presented in Section 8.

5. Secrecy Methods for Enhancing Performance

In Section 2, the US method is used to choose the operating transmitter, assuming each LED has an equal probability of being selected. However, this method is not always optimal. New transmitter selection strategies are introduced here to enhance the secrecy rate.

5.1. Channel-Adaptive Selection Technique

In this technique, the possibility of picking every LED varies depending on both Bob and Eve's CSI. The rate of secrecy goes up as the difference between $h_{B,m}/\sigma_B$ and $h_{E,m}/\sigma_E$ grows larger. To increase the rate of secrecy, the LED with a large $h_{B,m}/\sigma_B - h_{E,m}/\sigma_E$ should be chosen with a high probability. Therefore, in (2), the probability of choosing the m-th LED is changed as [44]

$$p(h_k = h_{k,m}) = \frac{\frac{h_{B,m}}{\sigma_B} - \frac{h_{E,m}}{\sigma_E}}{\sum_{j=1}^{M}\left(\frac{h_{B,m}}{\sigma_B} - \frac{h_{E,m}}{\sigma_E}\right)}, \; k = B \text{ or } E \tag{35}$$

Algorithm 1 [44] details the practical selection process of each LED in the CAS system. Assuming there are N time intervals, the computational complication of Algorithm 1 is $O(MN)$, making the CAS technique computationally efficient. Additionally, since $0 \leq q_i \leq 1$ for all $i \in \{1, \ldots, M\}$ and $r \in [0, 1]$, Steps $6-10$ are used to select a specific LED. LEDs can be selected independently at various time points, ensuring that *Algorithm 1* is convergent. *Theorems 1* and *2* can be reformulated as *Theorem 5* using the CAS technique.

Algorithm 1 The CAS technique

1: **Input:** σ_B, σ_E, and M.
2: **Output:** The k-th index of LED.
3: Get Alice's, Bob's, and Eve's locations.
4: Calculate the probability of every LED being selected utilizing (35).
5: Calculate the accumulated probability of $q_i = \sum_{m=1}^{i} p(h_k = h_{k,m})$, $i = 1, \ldots, M$.
6: Produce a randomly generated r in the interval $[0, 1]$.
7: **if** $r < q_1$ then
8: The 1st index is chosen.
9: else if $q_{k-1} < r < q_k$ then
10: The k-th index is chosen.
11: **end if**
12: Iterate the above steps $2-10$ for choosing a different index for the subsequent particular time.

Theorem 5. *Utilizing the CAS technique in (35), we can find the lower and upper bounds of the secrecy rate for the SM-based VLC subject to constraints (3) and (5) as follows:*

$$R_s \geq \sum_{m=1}^{M} \left\{ \frac{\frac{h_{B,m}}{\sigma_B} - \frac{h_{E,m}}{\sigma_E}}{\sum_{j=1}^{M}\left(\frac{h_{B,m}}{\sigma_B} - \frac{h_{E,m}}{\sigma_E}\right)} \left\{ \frac{1}{2} ln\left[\frac{e\xi^2 P^2 \sigma_E^2}{2\pi\sigma_B^2\left(h_{E,m}^2 \xi^2 P^2 + h_{E,m}\xi P \varsigma_E^2 \sigma_E^2 + \sigma_E^2\right)} \right] + f_{low}(h_{B,m}, \xi, P) + \right. \right.$$
$$\left. \left. \frac{1}{2}\left[e^{\frac{1}{h_{B,m}\varsigma_B^2 \xi P}} \mathbb{E}i\left(-\frac{1}{h_{B,m}\varsigma_B^2 \xi P}\right) - e^{\frac{1}{h_{E,m}\varsigma_E^2 \xi P}} \mathbb{E}i\left(-\frac{1}{h_{E,m}\varsigma_E^2 \xi P}\right) \right] \right\} \right\}. \tag{36}$$

$$R_s \leq \begin{cases} \sum_{m=1}^{M} \left\{ \frac{\frac{h_{B,m}}{\sigma_B} - \frac{h_{E,m}}{\sigma_E}}{\sum_{j=1}^{M}\left(\frac{h_{B,m}}{\sigma_B} - \frac{h_{E,m}}{\sigma_E}\right)} \left[\ln\left(\sqrt{\frac{4eh_{E,m}\varsigma_E^2\sigma_E^2}{\pi^2 M}} + \sqrt{\frac{2e\xi P h_{B,m} h_{E,m}\varsigma_E^2\sigma_E^2}{\pi M \varsigma_B^2\sigma_B^2}} \right) \right] \right\} \\ \qquad \text{if } \frac{1}{\sqrt{2\pi}} \geq \frac{h_{E,m}}{h_{B,m}} \left(\sqrt{\frac{h_{B,m}\varsigma_B^2\sigma_B^2}{2\pi M}} + \frac{h_{B,m}}{2}\sqrt{\frac{\xi P}{M}} \right) \\ \frac{1}{2}\sum_{m=1}^{M} \left\{ \frac{\frac{h_{B,m}}{\sigma_B} - \frac{h_{E,m}}{\sigma_E}}{\sum_{j=1}^{M}\left(\frac{h_{B,m}}{\sigma_B} - \frac{h_{E,m}}{\sigma_E}\right)} \ln\left(\frac{4eh_{B,m}\varsigma_E^2\sigma_E^2}{\pi^2 h_{E,m}\varsigma_B^2\sigma_B^2} \right) \right\}, \text{ otherwise.} \end{cases} \tag{37}$$

Theorems 3 and *4* can be updated using the CAS approach as detailed in (35).

Theorem 6. *Applying the CAS technique outlined in (35), we can use (27) to calculate the lower bound of the secrecy rate for SM-based VLC with constraints (3)–(5), where* R_{s1} *and* R_{s2} *are expressed in (38), and the upper bound of the secrecy rate is given in (39).*

$$\begin{aligned} R_{s1} = \sum_{m=1}^{M} \Bigg\{ & \frac{\frac{h_{B,m}}{\sigma_B} - \frac{h_{E,m}}{\sigma_E}}{\sum_{j=1}^{M}\left(\frac{h_{B,m}}{\sigma_B} - \frac{h_{E,m}}{\sigma_E}\right)} \left(f_{low}(h_{B,m}, \xi, P) + \frac{1}{2} ln \left[\frac{6A^2\sigma_E^2}{\pi e \sigma_B^2 \left(h_{E,m}^2 A^2 + 6A h_{E,m}\varsigma_E^2\sigma_E^2 + 12\sigma_E^2 \right)} \right] + \right. \\ & \left. \frac{1}{2} ln \left(\frac{1 + h_{E,m} A \varsigma_E^2}{1 + h_{B,m} A \varsigma_B^2} \right) - \frac{ln\left(1 + h_{B,m} A \varsigma_B^2\right)}{2A h_{B,m}\varsigma_B^2} + \frac{ln\left(1 + h_{E,m} A \varsigma_E^2\right)}{2A h_{E,m}\varsigma_E^2} \right) \Bigg\}, \end{aligned} \tag{38a}$$

$$\begin{aligned} R_{s2} = \sum_{m=1}^{M} \Bigg\{ & \frac{\frac{h_{B,m}}{\sigma_B} - \frac{h_{E,m}}{\sigma_E}}{\sum_{j=1}^{M}\left(\frac{h_{B,m}}{\sigma_B} - \frac{h_{E,m}}{\sigma_E}\right)} (f_{low}(h_{B,m}, \xi, P) \\ & + \frac{1}{2\left(e^{cA} - 1\right)} \Bigg\{ ln \left(\frac{1 + h_{E,m} A \varsigma_E^2}{1 + h_{B,m} A \varsigma_B^2} \right) e^{cA} - e^{-\frac{c}{h_{E,m}\varsigma_E^2}} \left[Ei\left(\frac{c}{h_{E,m}\varsigma_E^2} \left(1 + h_{E,m} A \varsigma_E^2\right) \right) - Ei\left(\frac{c}{h_{E,m}\varsigma_E^2} \right) \right] \\ & + e^{-\frac{c}{h_{B,m}\varsigma_B^2}} \left[Ei\left(\frac{c}{h_{B,m}\varsigma_B^2} \left(1 + h_{B,m} A \varsigma_B^2\right) \right) - Ei\left(\frac{c}{h_{B,m}\varsigma_B^2} \right) \right] \Bigg\} \\ & - \frac{1}{2} ln \left[2\pi e \left(h_{E,m}^2 \left(\frac{A(cA-2)}{c\left(1 - e^{-cA}\right)} + \frac{2}{c^2} - \xi^2 P^2 \right) + h_{E,m} \xi P \varsigma_E^2 \sigma_E^2 + \sigma_E^2 \right) \right] \Bigg) - c\xi P \\ & + \frac{1}{2} ln \left(\frac{\sigma_E^2}{\sigma_B^2} \frac{\left(e^{cA} - 1\right)^2}{c^2} \right) \Bigg\} \end{aligned} \tag{38b}$$

$$R_s \leq \frac{1}{2} \sum_{m=1}^{M} \left\{ \frac{\frac{h_{B,m}}{\sigma_B} - \frac{h_{E,m}}{\sigma_E}}{\sum_{j=1}^{M}\left(\frac{h_{B,m}}{\sigma_B} - \frac{h_{E,m}}{\sigma_E}\right)} \cdot \ln \left[\frac{h_{E,m}\varsigma_E^2\sigma_E^2\left(h_{B,m}A + \varsigma_B^2\sigma_B^2\right)}{\varsigma_B^2\sigma_B^2\left(h_{E,m}^2 A + \frac{h_{E,m}^2}{h_{B,m}}\varsigma_B^2\sigma_B^2 + M\right)} \right] \right\}, \tag{39}$$

5.2. Greedy Selection Technique

This subsection introduces the GS method. At each time instant, the LED with the highest value of $h_{B,m}/\sigma_B - h_{E,m}/\sigma_E$ is selected. The probability of choosing the m-th LED is then [44]

$$p(h_k = h_{k,m}) = \begin{cases} 1, & \text{if } m = \arg\max\limits_{k=1,\ldots,M} \left(\frac{h_{B,m}}{\sigma_B} - \frac{h_{E,m}}{\sigma_E} \right) \\ 0, & \text{otherwise,} \end{cases} \tag{40}$$

Algorithm 2 [44] outlines the process for selecting each LED using this technique. With a computational complexity of $O(MN)$, similar to Algorithm 1, the GS method is also efficient. Additionally, since the value $h_{B,k}/\sigma_B - h_{E,k}/\sigma_E$ varies with k, the index m can be determined for each time instant using $m = \arg\max\limits_{k=1,\ldots,M} \left(\frac{h_{B,m}}{\sigma_B} - \frac{h_{E,m}}{\sigma_E} \right)$. The LED selections at different time instants are independent. Therefore, *Algorithm 2* is convergent as well. *Theorems 1* and *2* can be updated to *Theorem 7* using the GS approach.

Algorithm 2 The GS technique

1: **Input:** σ_B, σ_E, and M.
2: **Output:** The m-th index of LED.
3: Get Alice's, Bob's, and Eve's locations.
4: Calculate $h_{B,k}/\sigma_B - h_{E,k}/\sigma_E$ for $k = 1, \ldots, M$.
5: **if** $m = \arg\max_{k=1,\ldots,M} \left(\frac{h_{B,m}}{\sigma_B} - \frac{h_{E,m}}{\sigma_E}\right)$ **then**
6: The m-th index is chosen.
7: **end if**
8: Iterate the above steps 2–6 for choosing a different index for the subsequent particular time.

Theorem 7. *For the SM-based VLC with constraints (3) and (5), the lower and upper secrecy rate bounds are given as*

$$R_s \geq \max_m \left\{ \frac{1}{2} ln \left[\frac{e\xi^2 P^2 \sigma_E^2}{2\pi\sigma_B^2 \left(h_{E,m}^2 \xi^2 P^2 + h_{E,m} \xi P \varsigma_E^2 \sigma_E^2 + \sigma_E^2\right)} \right] + f_{low}(h_{B,m}, \xi, P) + \frac{1}{2} \left[e^{\frac{1}{h_{B,m}\varsigma_B^2 \xi P}} \mathbb{E}i\left(-\frac{1}{h_{B,m}\varsigma_B^2 \xi P}\right) - e^{\frac{1}{h_{E,m}\varsigma_E^2 \xi P}} \mathbb{E}i\left(-\frac{1}{h_{E,m}\varsigma_E^2 \xi P}\right) \right] \right\}. \tag{41}$$

$$R_s \leq \begin{cases} \max_m \left\{ \ln\left(\sqrt{\frac{4eh_{E,m}\varsigma_E^2\sigma_E^2}{\pi^2 M}} + \sqrt{\frac{2e\xi P h_{B,m} h_{E,m} \varsigma_E^2 \sigma_E^2}{\pi M \varsigma_B^2 \sigma_B^2}} \right) \right\}, \\ \quad \text{if } \frac{1}{\sqrt{2\pi}} \geq \frac{h_{E,m}}{h_{B,m}} \left(\sqrt{\frac{h_{B,m}\varsigma_B^2\sigma_B^2}{2\pi M}} + \frac{h_{B,m}}{2} \sqrt{\frac{\xi P}{M}} \right) \\ \max_m \left\{ \frac{1}{2} \ln\left(\frac{4eh_{B,m}\varsigma_E^2\sigma_E^2}{\pi^2 h_{E,m}\varsigma_B^2\sigma_B^2} \right) \right\}, \text{ otherwise} \end{cases}, \tag{42}$$

GS technique updates *Theorems 3* and *4* to *Theorem 8*.

Theorem 8. *The lower and upper bounds for the secrecy rate in the SM-based VLC, subject to constraints (3)–(5) are provided by*

$$R_{s1} = \max_m \left\{ f_{low}(h_{B,m}, \xi, P) + \frac{1}{2} \ln\left[\frac{6A^2\sigma_E^2}{\pi e \sigma_B^2 \left(h_{E,m}^2 A^2 + 6A h_{E,m} \varsigma_E^2 \sigma_E^2 + 12\sigma_E^2\right)} \right] + \frac{1}{2} \ln\left(\frac{1 + h_{E,m} A \varsigma_E^2}{1 + h_{B,m} A \varsigma_B^2} \right) - \frac{\ln\left(1 + h_{B,m} A \varsigma_B^2\right)}{2A h_{B,m} \varsigma_B^2} + \frac{ln\left(1 + h_{E,m} A \varsigma_E^2\right)}{2A h_{E,m} \varsigma_E^2} \right\}, \tag{43a}$$

$$R_{s2} = \max_m \left\{ \left(f_{low}(h_{B,m}, \xi, P) + \frac{1}{2(e^{cA}-1)} \left\{ \ln\left(\frac{1 + h_{E,m} A \varsigma_E^2}{1 + h_{B,m} A \varsigma_B^2}\right) e^{cA} - e^{-\frac{c}{h_{E,m}\varsigma_E^2}} \left[Ei\left(\frac{c}{h_{E,m}\varsigma_E^2}\left(1 + h_{E,m} A \varsigma_E^2\right)\right) - Ei\left(\frac{c}{h_{E,m}\varsigma_E^2}\right) \right] + e^{-\frac{c}{h_{B,m}\varsigma_B^2}} \left[Ei\left(\frac{c}{h_{B,m}\varsigma_B^2}\left(1 + h_{B,m} A \varsigma_B^2\right)\right) - Ei\left(\frac{c}{h_{B,m}\varsigma_B^2}\right) \right] \right\} - \frac{1}{2} \ln\left[2\pi e \left(h_{E,m}^2 \left(\frac{A(cA-2)}{c(1-e^{-cA})} + \frac{2}{c^2} \right) - \xi^2 P^2 \right) + h_{E,m} \xi P \varsigma_E^2 \sigma_E^2 + \sigma_E^2 \right] \right) - c\xi P + \frac{1}{2} \ln\left(\frac{\sigma_E^2}{\sigma_B^2} \frac{\left(e^{cA}-1\right)^2}{c^2} \right) \right\}. \tag{43b}$$

$$R_s \leq \max_m \left\{ \frac{1}{2} \ln \left[\frac{h_{E,m} \varsigma_E^2 \sigma_E^2 \left(h_{B,m} A + \varsigma_B^2 \sigma_B^2\right)}{\varsigma_B^2 \sigma_B^2 \left(h_{E,m}^2 A + \frac{h_{E,m}^2}{h_{B,m}} \varsigma_B^2 \sigma_B^2 + M \right)} \right] \right\}, \tag{44}$$

6. Secrecy-Rate Enhancement-Based Optical Jamming

The friendly jamming technique can enhance the secrecy rate of SM-based VLC systems. In standard SM, one LED out of M is active for communication while the remaining $M-1$ LEDs are idle. By utilizing friendly jamming, these inactive LEDs can be used to

emit optical jamming signals to increase noise for eavesdroppers. Assuming Alice lacks the CSI of a passive eavesdropper, she can transmit an optical jamming signal in the null-space of the main channel, alongside the information signal. When Alice uses the m-th LED for transmission, the other $M-1$ LEDs can simultaneously send jamming signals without interfering with Bob's reception. Bob receives the intended information as usual, while Eve faces interference from Alice's jamming. However, enhancing secrecy performance necessitates deploying additional LEDs and allocating extra power for jamming, all while maintaining equal power levels. By employing singular value decomposition [38], the VLC gain of the main channel h_B can be expressed as

$$\mathbf{h_B^T} = \left[\lambda, \mathbf{0^T}\right][\mathbf{v_s}, \mathbf{V_n}]^{\mathrm{T}}, \tag{45}$$

where λ and $\mathbf{v_s}$ represent the singular value and the right singular vector of the VLC channel gain h_B, respectively. Based on (45), a null space $\mathbf{V_n} = [\mathrm{v_s}, \mathrm{v_s}, \cdots, \mathrm{v}_{M-1}] \in R^{M\times(M-1)}$ is identified, given that h_B has $\mathrm{rank}(h_B) = 1$. Consequently, the optical jamming generated by Alice is formulated as

$$\mathbf{w} = \mathbf{V_n}\mathbf{u}, \tag{46}$$

where $\mathbf{u}$ is a time-varying jamming vector with elements following a real truncated Gaussian distribution [47] within the range $\left[\frac{-A_2}{M-1}, \frac{A_2}{M-1}\right]$. Thus, the peak amplitude constraint for the $(M-1)$ jamming codewords is $[-A_2, +A_2]$, and for the private signal, it is A_1. The total peak amplitude constraint for the LEDs is therefore $A = A_1 + A_2$.

The total noise at Bob and Eve includes both signal-independent and signal-dependent components [11]. When the m-th LED is selected for transmission, the signals received by Bob and Eve are given as

$$\begin{cases} Y_B = h_{B,m}X + \sqrt{h_{B,m}X}Z_{B,1} + Z_{B,0} \\ Y_E = h_{E,m}X + \sqrt{h_{E,m}X}Z_{E,1} + \mathbf{h_E^T}\mathbf{w} + Z_{E,0} \end{cases}, \tag{47}$$

where $Z_{B,1} \sim \mathcal{N}\left(0, \varsigma_B^2\sigma_B^2\right)$ and $Z_{E,1} \sim \mathcal{N}\left(0, \varsigma_E^2(\sigma_E^2 + \sigma_W^2)\right)$ and σ_W^2 is the noise power at Eve due to optical jamming. $\mathbf{h_E^T}$ is the VLC gain of the wiretap channel, and $(h_{B,m}, h_{E,m})$ are the instant channel gain between the selected m-th LED and the PD of Bob and Eve respectively.

Bob's reception is unaffected by the optical jamming produced by $\mathbf{w}$, aside from a portion of power being allocated to it. However, Eve's reception may be significantly disrupted, enhancing Bob's secrecy performance, as shown in the simulations.

Let $\check{Z}_{E,0}$ represent the noise experienced by Eve. According to (42), we have

$$\check{Z}_{E,0} = \mathbf{h_E^T}\mathbf{w} + Z_{E,0} = \mathbf{h_E^T}\mathbf{V_n}\mathbf{u} + Z_{E,0} = \sum_{i=1}^{M-1} u_i\mathbf{h_E^T}\mathrm{v_i} + Z_{E,0}, \tag{48}$$

This represents the sum of $M-1$ independently distributed variables with varying variances. Finding a closed-form PDF for $\check{Z}_{E,0}$, derived from the convolution of double-sided truncated Gaussian variables, is challenging. Therefore, we use the Lyapunov central limit theorem, which states that the sum of T independent variables approximates a Gaussian distribution as T increases. With more than ten LEDs typically used in practice, the theorem's approximation of independent truncated Gaussian variables as Gaussian is suitable for our VLC systems. Thus, $\check{Z}_{E,0}$ is approximately Gaussian.

The Gaussian approximation simplifies the assertion that $\check{Z}_{E,0}$ has a mean of zero and a variance of

$$\begin{aligned}\Omega_{\mathrm{E}}^2 &= \mathbb{E}\left\{\left(\mathbf{h}_{\mathrm{E}}^{\mathbf{T}}\sum_{i=1}^{M-1}u_i\mathrm{v}_i\right)\left(\mathbf{h}_{\mathrm{E}}^{\mathbf{T}}\sum_{j=1}^{M-1}u_j\mathrm{v}_j\right)^T\right\}+\sigma_E^2\\ &= \tfrac{\sigma_J^2}{M-1}\mathbf{h}_{\mathrm{E}}^{\mathbf{T}}\left(\sum_{i=1}^{M-1}\mathrm{v}_i\mathrm{v}_i^T\right)\mathbf{h}_{\mathrm{E}}+\sigma_E^2 = \tfrac{\sigma_J^2}{M-1}\mathbf{h}_{\mathrm{E}}^{\mathrm{T}}\mathbf{V}_{\mathrm{n}}\mathbf{V}_{\mathrm{n}}^{\mathrm{T}}\mathbf{h}_{\mathrm{E}}+\sigma_E^2,\\ &= \sigma_W^2+\sigma_E^2,\end{aligned} \tag{49}$$

where σ_J^2 is the power of the optical jamming. This equality is obtained based on the statistical independence of $\{u_i\}_{i=1}^{M-1}$ and $Z_{E,0}$. When optical jamming is applied, Equations (14)–(44) can be applied with σ_E^2 replaced by $\left(\sigma_W^2+\sigma_E^2\right)$.

7. Scenarios with Multiple Receivers

In this section, we analyze scenarios involving multiple legitimate receivers and illegitimate receivers (adversary). For generality, we assume the presence of U legitimate receivers and V adversaries. The signals received by each legitimate receiver and adversary are expressed as follows:

$$\begin{cases} Y_{B,u} = h_{B,u,m}X+\sqrt{h_{B,u,m}X}Z_{B,u,1}+Z_{B,u,0}, & u\in\{1,2,\dots U\}\\ Y_{E,v} = h_{E,v,m}X+\sqrt{h_{E,v,m}X}Z_{E,v,1}+Z_{E,v,0}, & v\in\{1,2,\dots V\}\end{cases} \tag{50}$$

where $Z_{B,u,0}\sim\mathcal{N}\left(0,\sigma_{E,u}^2\right)$ and $Z_{E,v,0}\sim\mathcal{N}\left(0,\sigma_{E,v}^2\right)$ represent the signal-independent noise at the u-th legitimate receiver and v-th adversary, respectively. Similarly, $Z_{B,u,1}\sim\mathcal{N}\left(0,\varsigma_{B,u}^2\sigma_{B,u}^2\right)$, $Z_{E,v,1}\sim\mathcal{N}\left(0,\varsigma_{E,v}^2\sigma_{E,v}^2\right)$ denote the signal-dependent noise at the u-th legitimate receiver and v-th adversary, respectively.

We assume that the adversaries do not collude, meaning each processes their received signals independently. The adversary with the highest mutual information is considered the worst-case adversary. The secrecy rate R_s for the u-th legitimate receiver, as defined in (6) and (25), becomes

$$\begin{aligned}&R_{s,u} = \max_{f_X(x)}[I(X,h_{B,u};Y_{B,u})-I(X,h_E;Y_E)],\\ &\text{where}\\ &I(X,h_E;Y_E) = \max_{v=\{1,2,\dots V\}}I(X,h_{E,v};Y_{E,v}).\end{aligned} \tag{51}$$

Thus, the secrecy capacity is formulated according to problems (6) and (25). This confirms that the secrecy capacity bounds obtained in Sections 3–5 remain valid in scenarios with multiple receivers, assuming non-colluding adversaries.

8. Numerical Results

In this section, we conduct numerical analyses of the indoor SM-based VLC system's secrecy rate. Assuming a three-node indoor VLC system with a 5 m × 4 m × 3 m room. $M = 4$ LEDs (Alice) are mounted on the 3 m ceiling, whereas Bob and Eve are at 0.8 m. Table 1 displays Alice and Bob's coordinates. Bob and Eve's noise variances are selected to be $\sigma_B^2 = \sigma_E^2 = 1$ and $\varsigma_B^2 = \varsigma_E^2 = 1.5$.

Table 1. Location of Alice and Bob.

	Alice	**Bob**
Locations	(1.8, 1.8, 3), (2.2, 1.8, 3), (1.8, 2.2, 3), (2.2, 2.2, 3)	(1.95, 1.95, 0.75)

8.1. SM-Based VLC with Constraints (3) and (5)

The secrecy rate bounds vs. P with varied h_B/h_E when $\xi = 0.3$ are shown in Figure 3 for various noise conditions. Every secrecy rate bound in this figure grows as h_B/h_E and P increase. However, when P grows, they tend to take on more stable values. Furthermore, with signal-dependent (SD) noise, the secrecy rate bounds are lower than with signal-independent (SID) noise. This demonstrates that the presence of signal-dependent noise reduces VLC's secrecy rate. In order to quantify the gaps between the upper (14) and lower (22) bounds of secrecy rate with signal-dependent noise in the region of high optical intensity, Table 2 is presented. All performance gaps are approximately 0.467 Nat/transmission, as may be noticed. This finding is the same as that stated in Remark 1.

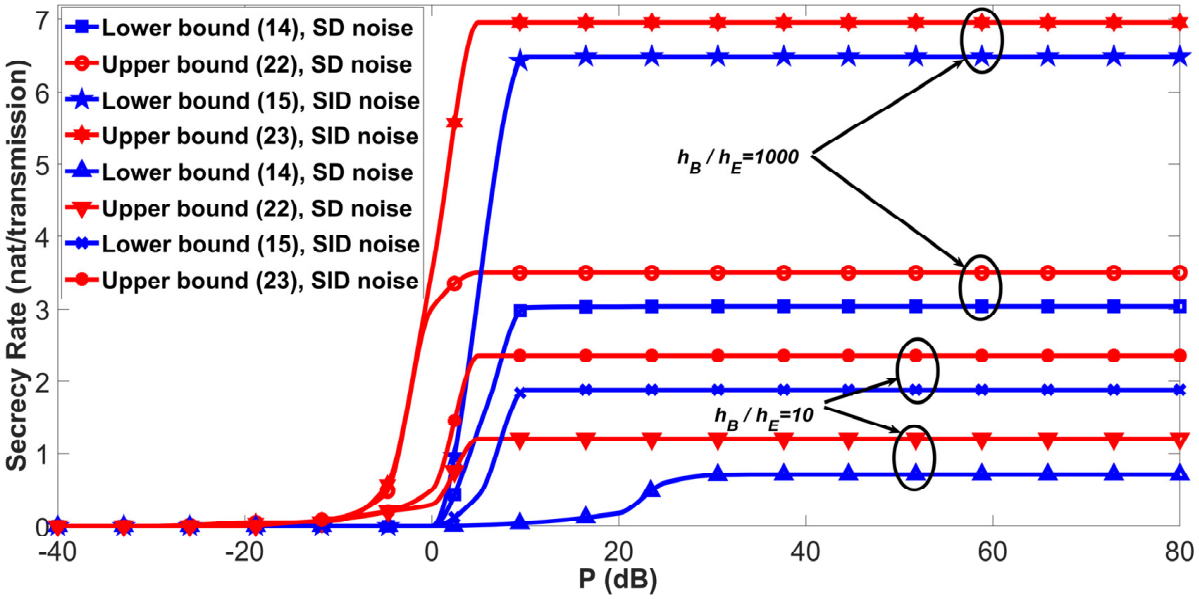

Figure 3. Secrecy rate bounds vs. P for varying h_B/h_E and $\xi = 0.3$.

Table 2. Performance gaps between (14) and (22) at high SNR.

P (dB)	h_B/h_E=10	h_B/h_E=1000
65	0.468	0.467
70	0.467	0.467
75	0.467	0.4672

Figure 4 illustrates the link between the secrecy rate bounds and ξ for varying P, with $h_B/h_E = 1000$ under various noise conditions. For small values of ξ, increasing ξ results in a swift escalation in the secrecy rate bounds. Nevertheless, as ξ increases, the secrecy rate bounds tend to stabilize. In addition, when P increases, so does the performance of the secrecy rate. This suggests that an indoor VLC system with a greater nominal optical intensity outperforms. Additionally, Figure 4 illustrates that the secrecy rate bounds with signal-dependent noise are lower than with signal-independent noise. This also demonstrates that the presence of signal-dependent noise reduces VLC's secrecy rate.

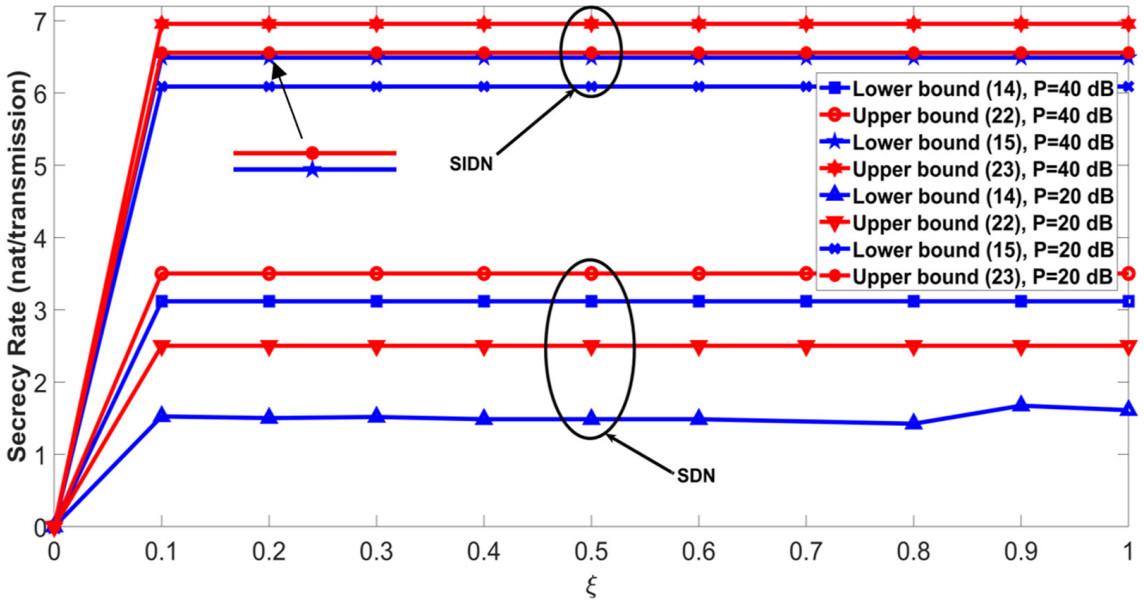

Figure 4. Secrecy rate bounds vs. ξ for varying P and $h_B/h_E = 1000$.

8.2. SM-Based VLC with Constraints (3)–(5)

Figure 5 illustrates the secrecy rate bounds vs. P with varying h_B/h_E when $A = P$. Particularly, Figure 5 displays the results when $\xi = 0.5$. Much like Figure 3, the secrecy rate bounds exhibit initial growth before eventually stabilizing as P rises. In addition, the secrecy rates improve when h_B/h_E increases. The performance disparities between the lower bound (27) and the upper bound (32) are insignificant. In order to quantify these differences at high SNR with $\xi = 0.5$, refer to Table 3. Consistent with the conclusion in Remark 3, there is a performance gap of roughly 0.1765 Nat/transmission between the asymptotic lower bound and the asymptotic upper bound of secrecy rates. Figure 5 shows that signal-dependent noise has lower secrecy rate bounds than signal-independent noise. Signal-dependent noise affects VLC's secrecy rate.

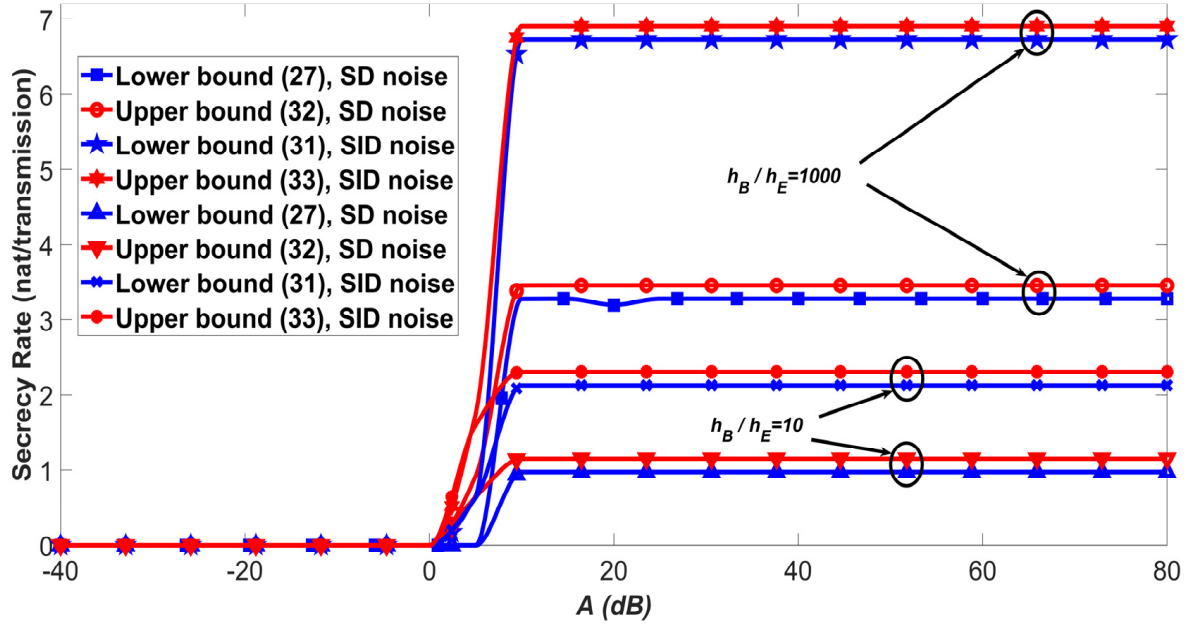

Figure 5. Secrecy rate bounds vs. A for varying h_B/h_E when $\xi = 0.5$, $\alpha = 0.5$, and $A = P$.

Table 3. Performance gaps between (27) and (32) at high SNR.

P (dB)	h_B/h_E=10	h_B/h_E=1000
65	0.1765	0.1765
70	0.1765	0.1765
75	0.1765	0.1765

8.3. SM-Based VLC with the US, CAS, and GS Techniques

Given Alice's position, the locations of Bob and Eve impact the effectiveness of transmitter selection techniques. To compare the performance of the US, CAS, and GS methods, the mean secrecy rate is analyzed. Bob's position varies across the receiver plane, while Eve's position is fixed with $h_B/h_E = 1000$. Using the constraints (3) and (5), Figure 6 illustrates the mean secrecy rate bounds versus P for the three transmitter selection strategies with $\xi = 0.3$ and $h_B/h_E = 1000$. The GS scheme achieves the highest secrecy rate, followed by the CAS system and the US scheme, which achieves the lowest secrecy rate. This indicates that selecting a transmitter uniformly may not be the most effective strategy in a practical SM system. The GS and CAS schemes offer significant improvements in secrecy performance compared to the US approach.

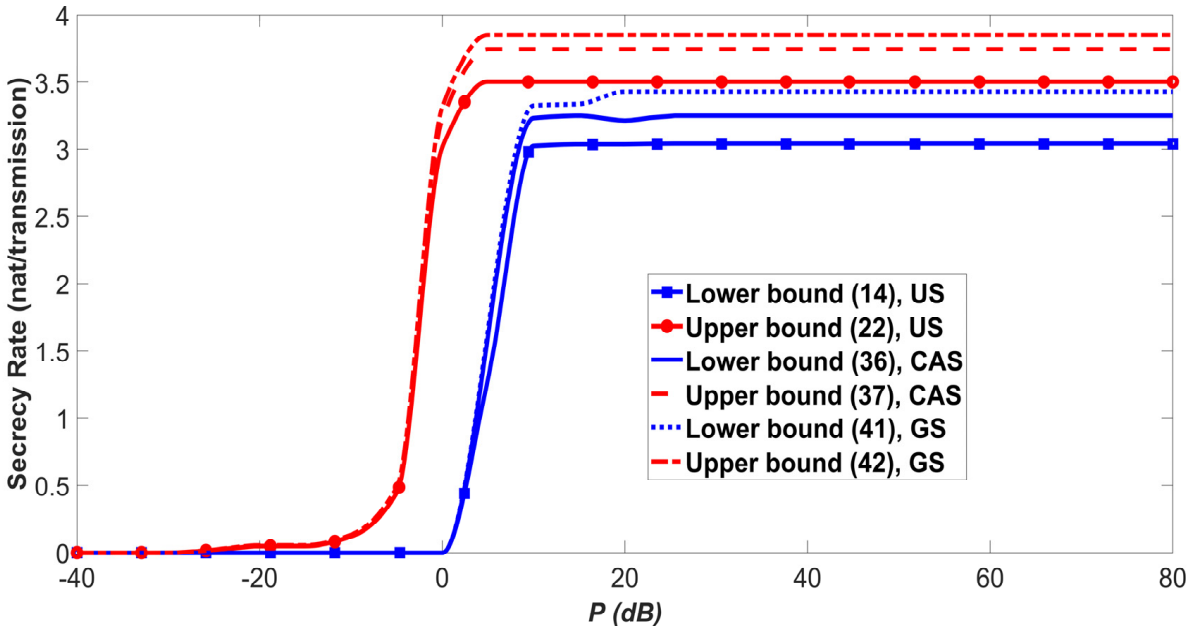

Figure 6. Secrecy rate bounds vs. P with $h_B/h_E = 1000$ and $\xi = 0.3$.

Using the constraints (3)–(5), Figure 7 illustrates the mean secrecy rate bounds versus P for the three transmitter selection strategies with $\xi = 0.5$, $\alpha = 0.5$, $A = P$, and $h_B/h_E = 1000$. As with Figure 6, the GS strategy provides the highest rate of secrecy, while the US scheme yields the lowest.

8.4. SM-Based VLC with Optical Jamming

Figure 8 illustrates the effect of optical jamming on the enhancement of the secrecy rate in both signal-dependent noise and signal-independent noise scenarios at $h_B/h_E = 100$, $\xi = 0.5$, and $A = P$. As depicted, in both signal-dependent noise and signal-independent noise scenarios without the application of optical jamming, an increase in P leads to a steady improvement in secrecy rates. However, when optical jamming is introduced, the secrecy rate shows a slower increase within a limited range of P, similar to the scenario without jamming. Notably, once $P \geq 45$ dB, the introduction of AN causes the secrecy

rate to rise more rapidly. This demonstrates that the use of friendly optical jamming significantly enhances the secrecy rate, especially in scenarios with high optical power, such as $P \geq 45$ dB. At $P = 80$ dB, there is an approximate increase of 3.9 nat/transmission compared to the scenario without optical jamming in both signal-dependent noise and signal-independent noise scenarios. Furthermore, as indicated in earlier results, secrecy is more effectively enhanced using signal-independent noise compared to signal-dependent noise. Specifically, at $P = 80$ dB, the inclusion of signal-independent noise results in an approximate increase of 3.5 nat/transmission compared to signal-dependent noise, underscoring the detrimental impact of signal-dependent noise on the achievable secrecy rate in VLC systems.

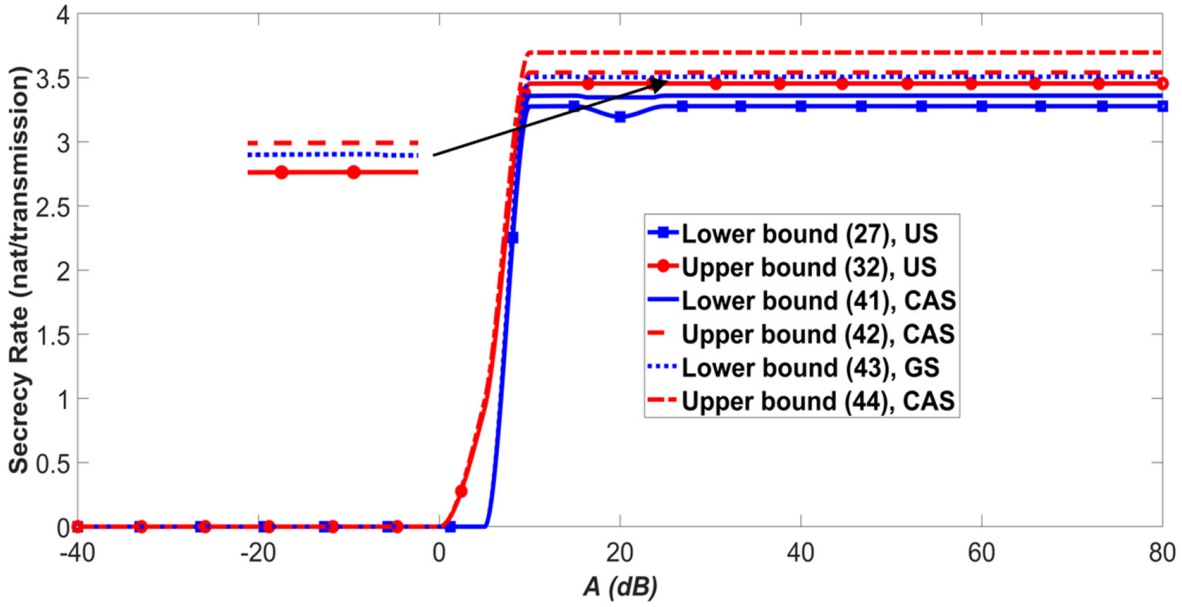

Figure 7. Secrecy rate bounds vs. A with $h_B/h_E = 1000$ when $\xi = 0.5$, $\alpha = 0.5$, and $A = P$.

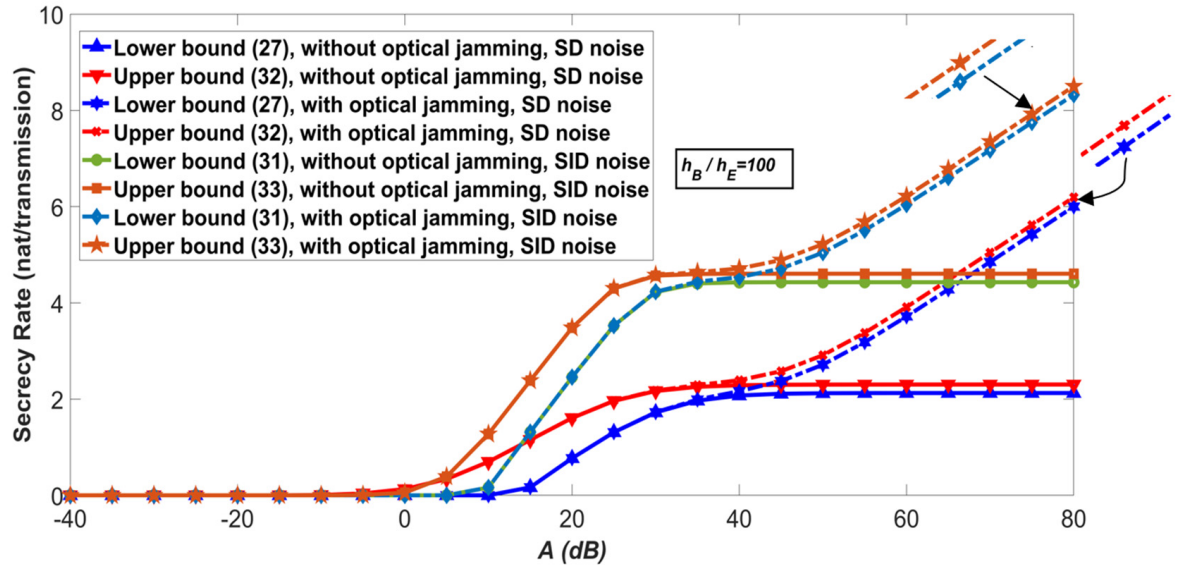

Figure 8. Secrecy rate bounds with/without optical jamming vs. A, $h_B/h_E = 100$, $\xi = 0.5$, $A = P$.

9. Discussion

This study presents an in-depth analysis of the secrecy rate in SM-based VLC systems, focusing on the effects of signal-dependent noise and proposing new methods to enhance physical-layer security. The results demonstrate that signal-dependent noise plays a significant role in limiting the secrecy performance of VLC systems. By deriving both lower and upper bounds for the secrecy rate under non-negativity, average, and peak optical intensity constraints, we found that signal-dependent noise substantially reduces the achievable secrecy rate compared to systems with signal-independent noise. At high optical intensity levels, the bounds converge, with the performance gap remaining minimal (approximately 0.1765 nat/transmission). Numerical findings also show that employing GS technique for transmitter selection results in better secrecy performance than the CAS and US methods. Furthermore, optical jamming proves highly effective in enhancing secrecy, particularly at higher power levels.

In comparing this study with previous works, several key differences emerge. While numerous studies have investigated secrecy in VLC systems, the majority, including works referenced [11–38], primarily assumed signal-independent noise, which is an unrealistic assumption for practical VLC scenarios. In contrast, the work in [39] and [40] addressed secrecy performance in VLC systems under signal-dependent noise, providing a more realistic analysis but applied in SISO systems. Moreover, while studies in [41–45] explored the confidentiality of VLC in SM systems, they primarily considered signal-independent noise, which is less practical for VLC systems.

The contribution of this study lies in its focus on SM-based VLC systems, which are less frequently analyzed in the context of signal-dependent noise. The incorporation of transmitter selection techniques (US, CAS, and GS) and optical jamming represents a significant advancement. Unlike earlier research that largely overlooked these aspects, our approach integrates adaptive selection techniques and optical jamming to enhance secrecy performance, particularly in high optical power scenarios. This study also extends the analysis to a three-indoor SM-based VLC scheme, accounting for signal-dependent noise and suggesting random noise variances at both the intended user and the adversary.

Table 4 provides a clear comparison of this study with recent works, highlighting the unique contributions of our approach. The distinction lies in addressing signal-dependent noise and leveraging advanced selection techniques and optical jamming, which were not extensively explored in prior research on SM-based VLC systems.

Table 4. Comparison of the recent works.

References	Noise Assumption	Secrecy Rate Bounds	Selection Techniques	Optical Jamming	Main Contribution
[11–14]	Signal-independent	Derived for SISO VLC	None	Not considered	Tight upper and lower bounds for secrecy capacity in SISO systems
[15–19]	Signal-independent	Secrecy sum rates, 3D networks	Not specified	Not considered	Physical-layer security in multi-user VLC networks
[20–25]	Signal-independent	Secrecy rate under secure beamforming	Not specified	Not considered	Secure beamforming in MISO VLC under CSI constraints
[26–31]	Signal-independent	Secrecy rate maximization using jamming	Not specified	Jamming used	Jamming and AN-aided precoding to improve secrecy
[32,33]	Signal-independent	Secrecy rate under secure beamforming and jamming	Not specified	Jamming used	Secure beamforming in MISO VLC under CSI constraints

Table 4. *Cont.*

References	Noise Assumption	Secrecy Rate Bounds	Selection Techniques	Optical Jamming	Main Contribution
[34–38]	Signal-independent	Secret-key derivation	Not specified	Not considered	Key generation from physical-layer signals
[39,40]	Signal-dependent	Secrecy performance in SISO VLC	Not specified	Jamming used	Investigate the secrecy rate for SISO VLC under signal-dependent noise
[41]	Signal-independent	Secrecy rate bounds in SM VLC	Not specified	Not considered	Investigate the secrecy rate for SM-based VLC systems
[42]	Signal-independent	Secrecy rate bounds in SM VLC	Not specified	Jamming used	Optical jamming scheme for enhancing secrecy in SM-VLC systems
[43,44]	Signal-independent	Secrecy rate bounds in SM VLC	US, CAS, GS	Not considered	Improve secrecy rate for SM-VLC using transmitter selection
This work	Signal-dependent	Secrecy rate bounds in SM VLC	US, CAS, GS	Jamming used	Improve secrecy rate for SM-VLC using transmitter selection and optical jamming under signal-dependent noise

The theoretical implications of this study are significant, as it advances the understanding of physical-layer security in VLC systems. The derived closed-form expressions for secrecy rate bounds provide a solid theoretical foundation for further exploration of SM-based VLC under signal-dependent noise. Moreover, this study extends current transmitter selection strategies by demonstrating the superior performance of the GS method, particularly in challenging noise environments. The use of optical jamming adds an innovative dimension to VLC security, offering a practical solution for enhancing secrecy, especially at high optical power levels. These contributions refine and extend existing theories on physical-layer security in VLC, providing new tools for addressing confidentiality in future wireless systems.

10. Conclusions

This study investigates the secrecy of indoor VLC systems utilizing the SM technique. The system comprises M transmitters, a receiver, and an adversary. In SM, only one transmitter is active at a time, and the US method is used to choose the active transmitter. We derive both lower and upper bounds on the secrecy rate under constraints of non-negativity and average optical intensity. Additional bounds are obtained by examining peak optical intensity. We also derive secrecy rate bounds for scenarios with only signal-independent noise by letting the signal-dependent noise variance approach zero.

When SNR is high, the performance gap between the lower and upper asymptotic bounds is minimal (approximately 0.1765 nat/transmission). Numerical findings reveal that signal-dependent noise significantly impacts the secrecy rate, which affects overall secrecy performance. Interestingly, the secrecy rate does not increase with P or A at high SNR levels; instead, it remains approximately constant. The CAS and GS schemes are employed to further enhance secrecy performance.

Furthermore, the impact of friendly optical jamming on the secrecy rate is examined. Results indicate that optical jamming significantly improves the secrecy rate at higher power levels. Specifically, at $P = 80$ dB, optical jamming enhances the secrecy rate by approximately 3.9 nat/transmission compared to scenarios without jamming.

In future work, we plan to delve into the analysis of the secrecy rate within VLC systems, utilizing advanced SM techniques such as generalized spatial modulation (GSM) and quadrature spatial modulation (QSM). These methodologies will be scrutinized in terms of their efficacy in enhancing the secrecy rate, juxtaposed against the conventional SM approach.

Author Contributions: Y.M.A.-M.: conceived the idea, generated the simulation results, and revised the manuscript. A.H.A.: discussed the results and revised the manuscript. M.T.A.: discussed the results and revised the manuscript. Y.A.-H.: discussed the results and revised the manuscript. All authors have read and agreed to the published version of the manuscript.

Funding: This work was supported by the King Saud University, Riyadh, Saudi Arabia, through Researchers Supporting Project number RSPD2024R1104.

Institutional Review Board Statement: Not applicable.

Informed Consent Statement: Not applicable.

Data Availability Statement: All the data related to these findings are included in the manuscript.

Conflicts of Interest: The authors declare that they do not have any conflicts of interest regarding the publication of this article.

Appendix A

Proof of lower bound (14) in *Theorem 1*:

Maximizing source entropy while adhering to constraints (3) and (5) gives a secrecy rate lower bound in (13), i.e.,

$$\begin{aligned} \max_{f_X(x)} \mathcal{H}(X) &= -\int_0^\infty f_X(x) ln[f_X(x)] \mathrm{d}x \\ \text{s.t. } &\int_0^\infty f_X(x) \mathrm{d}x = 1 \\ &\mathbb{E}(X) = \int_0^\infty x f_X(x) \mathrm{d}x = \xi P. \end{aligned} \tag{A1}$$

When we apply the variational method to the input X, we obtain an optimized PDF as follows:

$$f_X(x) = \frac{1}{\xi P} e^{-\frac{1}{\xi P}x}, x \geq 0. \tag{A2}$$

From (A2), we can obtain

$$\begin{cases} H(X) = ln(e\xi P) \\ \mathbb{E}_x(X) = \xi P \\ \mathrm{var}(X) = \xi^2 P^2 \\ \mathbb{E}_{X,Z_{E,1}}\left(\sqrt{X} Z_{E,1}\right) = \mathbb{E}_X\left(\sqrt{X}\right) \mathbb{E}_{Z_{E,1}}(Z_{E,1}) = 0 \\ \mathrm{var}(Y_E) = h_{E,m}^2 \xi^2 P^2 + h_{E,m} \xi P \varsigma_E^2 \sigma_E^2 + \sigma_E^2 \end{cases} \tag{A3}$$

Furthermore, $\mathbb{E}_x\left[\ln\left(\frac{1+h_{E,m}X\varsigma_E^2}{1+h_{B,m}X\varsigma_B^2}\right)\right]$ can be computed as [40]

$$\mathbb{E}_x\left[ln\left(\frac{1+h_{E,m}X\varsigma_E^2}{1+h_{B,m}X\varsigma_B^2}\right)\right] = \left[e^{\frac{1}{h_{B,m}\varsigma_B^2 \xi P}} \mathbb{E}i\left(-\frac{1}{h_{B,m}\varsigma_B^2 \xi P}\right) - e^{\frac{1}{h_{E,m}\varsigma_E^2 \xi P}} \mathbb{E}i\left(-\frac{1}{h_{E,m}\varsigma_E^2 \xi P}\right)\right]. \tag{A4}$$

Theorem 1 is obtained by substituting (A3) and (A4) into (13).

Appendix B

Proof of Upper bound (22) in *Theorem 2*:

Based on (21), the secrecy rate is upper-bounded as

$$R_s \le \frac{1}{M}\sum_{m=1}^{M}\left(\underbrace{\mathbb{E}_{X^*\dot{Y}_{E,m}}\{u_1\}}_{I_1} - \underbrace{\mathbb{E}_{X^*\dot{Y}_{E,m}}\{u_2\}}_{I_1}\right), \tag{A5}$$

where u_1 and u_2 are defined as follows:

$$\begin{aligned} u_1 &= \int_{-\infty}^{\infty} f_{\dot{Y}_{B,m}|X\dot{Y}_{E,m}}\left(\dot{y}_{B,m}\middle|X,\dot{Y}_{E,m}\right)\ln\left[f_{\dot{Y}_{B,m}|X\dot{Y}_{E,m}}\left(\dot{y}_{B,m}\middle|X,\dot{Y}_{E,m}\right)\right]d\dot{y}_{B,m},\\ u_2 &= \int_{-\infty}^{\infty} f_{\dot{Y}_{B,m}|X\dot{Y}_{E,m}}\left(\dot{y}_{B,m}\middle|X,\dot{Y}_{E,m}\right)\ln g_{\dot{Y}_{B,m}|\dot{Y}_{E,m}}\left(\dot{y}_{B,m}\middle|\dot{Y}_{E,m}\right)d\dot{y}_{B,m}. \end{aligned} \tag{A6}$$

I_1 in (A5) is expressed as

$$I_1 = -\left[\mathcal{H}\left(\dot{Y}_{B,m}\middle|X^*\right) + \mathcal{H}\left(\dot{Y}_{E,m}\middle|X^*,\dot{Y}_{B,m}\right) - \mathcal{H}\left(\dot{Y}_{E,m}\middle|X^*\right)\right], \tag{A7}$$

where $\mathcal{H}\left(\dot{Y}_{k,m}\middle|X^*\right)$ ($k = B$ for Bob and $k = E$ for Eve) is obtained by

$$\mathcal{H}\left(\dot{Y}_{k,m}\middle|X^*\right) = \mathbb{E}_{X^*}\left\{\frac{1}{2}\ln\left[2\pi e\left(1+h_{k,m}X\varsigma_k^2\right)\sigma_E^2\right]\right\}. \tag{A8}$$

The conditional PDF $f_{\dot{Y}_{E,m}|X\dot{Y}_{B,m}}\left(\dot{y}_{E,m}\middle|X,\dot{Y}_{B,m}\right)$ is expressed as [40]

$$f_{\dot{Y}_{E,m}|X\dot{Y}_{B,m}}\left(\dot{y}_{E,m}\middle|X,\dot{Y}_{B,m}\right) = \frac{1}{\sqrt{2\pi(MX+N)}}e^{-\frac{\left(\dot{y}_{E,m}-\frac{h_{E,m}}{h_{B,m}}\dot{Y}_{B,m}\right)}{2(MX+N)}}, \tag{A9}$$

where $M = h_{E,m}^2\varsigma_B^2\sigma_B^2/h_{B,m} + h_{E,m}\varsigma_E^2\sigma_E^2$ and $N = h_{E,m}^2\sigma_B^2/h_{B,m}^2 + \sigma_E^2$. According to the conditional PDF (A9), $\mathcal{H}\left(\dot{Y}_{E,m}\middle|X^*,\dot{Y}_{B,m}\right)$ can be obtained as

$$\mathcal{H}\left(\dot{Y}_{E,m}\middle|X^*,\dot{Y}_{B,m}\right) = \mathbb{E}_{X^*}\left\{\frac{1}{2}\ln[2\pi e(MX+N)]\right\}. \tag{A10}$$

Using (A8) and (A10), I_1 in (A7) is obtained as

$$I_1 = -\frac{1}{2}\ln\left(2\pi e\frac{\sigma_B^2}{\sigma_E^2}\right) - \frac{1}{2}\mathbb{E}_{X^*}\left\{\frac{1}{2}\ln(MN+N) + \ln\left(\frac{1+h_{B,m}X\varsigma_B^2}{1+h_{E,m}X\varsigma_E^2}\right)\right\}, \tag{A11}$$

For I_2 in (A5) to be computed, the conditional PDF $g_{\dot{Y}_{B,m}|\dot{Y}_{E,m}}\left(\dot{y}_{B,m}\middle|\dot{Y}_{E,m}\right)$ is selected as

$$g_{\dot{Y}_{B,m}|\dot{Y}_{E,m}}\left(\dot{y}_{B,m}\middle|\dot{Y}_{E,m}\right) = \frac{1}{2s^2}e^{-\frac{|\dot{y}_{B,m}-\mu\dot{y}_{E,m}|}{s^2}}, \tag{A12}$$

where s and μ are free parameters. Using (A12), I_2 is computed:

$$I_2 = \mathbb{E}_{X^*Y_{B,m}}\left\{\ln\left(2s^2\right) + \frac{1}{s^2}R_1\right\}, R_1 = \int_{-\infty}^{\infty}\frac{e^{-\frac{\left(\dot{y}_{E,m}-\frac{h_{E,m}}{h_{B,m}}\dot{Y}_{B,m}\right)^2}{2(MX+N)}}}{\sqrt{2\pi(MX+N)}}\left|\dot{Y}_{B,m}-\mu\dot{y}_{E,m}\right|d\dot{y}_{E,m}. \tag{A13}$$

Letting $t = \dot{y}_{E,m} - h_{E,m}\dot{Y}_{B,m}/h_{B,m}$ and utilizing the fact that $|a-b| \le |a| + |b|$, R_1 in (A13) can be written as

$$R_1 \le 2|\mu|\sqrt{\frac{MX+N}{2\pi}} + \left|1-\mu\frac{h_{E,m}}{h_{B,m}}\right|\left|\dot{Y}_{B,m}\right|. \tag{A14}$$

Using (A14), I_2 is written as

$$\begin{aligned} I_2 &= \mathbb{E}_{X^*}\left\{\ln\left(2s^2\right) + \tfrac{1}{s^2}\left[2|\mu|\sqrt{\tfrac{MX+N}{2\pi}} + \left|1-\mu\tfrac{h_{E,m}}{h_{B,m}}\right|R_2\right]\right\}, \\ R_2 &= \int_{-\infty}^{\infty} \tfrac{e^{-\frac{(\hat{y}_{B,m}-h_{B,m}X)^2}{2(1+h_{B,m}X\varsigma_B^2)\sigma_B^2}}}{\sqrt{2\pi\left(1+h_{B,m}X\varsigma_B^2\right)\sigma_B^2}}|\hat{y}_{B,m}|d\hat{y}_{B,m}. \end{aligned} \tag{A15}$$

From the fact $|a+b| \le |a| + |b|$, R_2 is upper-bounded by

$$R_2 \le 2\sqrt{\frac{\left(1+h_{B,m}X\varsigma_B^2\right)\sigma_B^2}{2\pi}} + h_{B,m}X. \tag{A16}$$

To obtain a tight upper bound, we initially take the partial derivative of (A15) with respect to s^2, resulting in I_2. The minimum point is

$$s^2 = 2|\mu|\sqrt{\frac{MX+N}{2\pi}} + \left|1-\mu\frac{h_{E,m}}{h_{B,m}}\right|R_2. \tag{A17}$$

Thus, I_2 is upper-bounded by

$$I_2 \le \mathbb{E}_{X^*}\left\{\ln\left[4e\left(|\mu|\sqrt{\frac{MX+N}{2\pi}} + \left|1-\mu\frac{h_{E,m}}{h_{B,m}}\right|\left(\sqrt{\frac{\left(1+h_{B,m}X\varsigma_B^2\right)\sigma_B^2}{2\pi}} + \frac{h_{B,m}X}{2}\right)\right)\right]\right\}, \tag{A18}$$

Substituting (A11) and (A18), R_s in (A5) can be computed in (A19). Utilizing the inequality $\frac{h_{B,m}X}{2\sqrt{MX+N}} \le \frac{h_{B,m}X}{2\sqrt{MX}} = \frac{h_{B,m}\sqrt{X}}{2\sqrt{M}}$ and the inequality of Jensen for convex functions $\ln(\cdot)$ and $\sqrt{\cdot}$, (A19) can be re-expressed in (A20).

$$\begin{aligned} R_s \le \tfrac{1}{M}\textstyle\sum_{m=1}^{M}\Bigg\{ &-\tfrac{1}{2}\ln\left(2\pi e\tfrac{\sigma_B^2}{\sigma_E^2}\right) - \tfrac{1}{2}\mathbb{E}_{X^*}\left[\ln\left(\tfrac{1+h_{B,m}X\varsigma_B^2}{1+h_{E,m}X\varsigma_E^2}\right)\right] + \mathbb{E}_{X^*}\Bigg[\ln\Bigg(4e\Bigg(\tfrac{|\mu|}{\sqrt{2\pi}} + \left|1-\mu\tfrac{h_{E,m}}{h_{B,m}}\right|\Bigg(\sqrt{\tfrac{\left(1+h_{B,m}X\varsigma_B^2\right)\sigma_B^2}{2\pi(MX+N)}} + \\ &\tfrac{h_{B,m}X}{2\sqrt{MX+N}}\Bigg)\Bigg)\Bigg)\Bigg]\Bigg\}. \end{aligned} \tag{A19}$$

$$\begin{aligned} R_s \le \tfrac{1}{M}\textstyle\sum_{m=1}^{M}\Bigg\{ &-\tfrac{1}{2}\ln\left(2\pi e\tfrac{\sigma_B^2}{\sigma_E^2}\right) - \tfrac{1}{2}\mathbb{E}_{X^*}\left[\ln\left(\tfrac{1+h_{B,m}X\varsigma_B^2}{1+h_{E,m}X\varsigma_E^2}\right)\right] + \mathbb{E}_{X^*}\Bigg[\ln\Bigg(4e\Bigg(\tfrac{|\mu|}{\sqrt{2\pi}} + \Bigg|1- \\ &\mu\tfrac{h_{E,m}}{h_{B,m}}\Bigg|\Bigg(\sqrt{\mathbb{E}_{X^*}\left[\tfrac{\left(1+h_{B,m}X\varsigma_B^2\right)\sigma_B^2}{2\pi(MX+N)}\right]} + \tfrac{h_{B,m}\sqrt{\xi P}}{2\sqrt{M}}\Bigg)\Bigg)\Bigg)\Bigg]\Bigg\}, \end{aligned} \tag{A20}$$

To satisfy illumination requirements, VLC systems operate with high optical intensity, and we are particularly focused on performance under such conditions. The optical input distribution tends to infinity as P approaches infinity [47]. Consequently, when P reaches infinity, we obtain

$$\begin{cases} \mathbb{E}_{X^*}\left[\ln\left(\tfrac{1+h_{B,m}X\varsigma_B^2}{1+h_{E,m}X\varsigma_E^2}\right)\right] = \tfrac{1+h_{B,m}P\varsigma_B^2}{1+h_{E,m}P\varsigma_E^2} \\ \mathbb{E}_{X^*}\left[\tfrac{\left(1+h_{B,m}X\varsigma_B^2\right)\sigma_B^2}{2\pi(MX+N)}\right] = \tfrac{\left(1+h_{B,m}P\varsigma_B^2\right)\sigma_B^2}{2\pi(MP+N)} \end{cases}. \tag{A21}$$

Furthermore, utilizing L'Hospital rule for (A21), we obtain

$$\begin{cases} \lim\limits_{P\to\infty}\tfrac{1+h_{B,m}P\varsigma_B^2}{1+h_{E,m}P\varsigma_E^2} = \tfrac{h_{B,m}\varsigma_B^2}{h_{E,m}\varsigma_E^2} \\ \lim\limits_{P\to\infty}\tfrac{\left(1+h_{B,m}P\varsigma_B^2\right)\sigma_B^2}{2\pi(MP+N)} = \tfrac{h_{B,m}\varsigma_B^2\sigma_B^2}{2\pi M} \end{cases}. \tag{A22}$$

Using (A21) and (A22), we rewrite (A20) as

$$R_s \le \frac{1}{M}\sum_{m=1}^{M}\left\{-\frac{1}{2}\ln\left(2\pi e\frac{h_{B,m}\varsigma_B^2\sigma_B^2}{h_{E,m}\varsigma_E^2\sigma_E^2}\right)+\left[\ln\left(4e\underbrace{\left(\frac{|\mu|}{\sqrt{2\pi}}+\left|1-\mu\frac{h_{E,m}}{h_{B,m}}\right|\left(\sqrt{\frac{h_{B,m}\varsigma_B^2\sigma_B^2}{2\pi M}}+\frac{h_{B,m}\sqrt{\xi P}}{2\sqrt{M}}\right)\right)}_{R_3}\right)\right]\right\} \tag{A23}$$

$$R_3=\mu\left[\frac{1}{\sqrt{2\pi}}-\frac{h_{B,m}}{h_{E,m}}\left(\sqrt{\frac{h_{B,m}\varsigma_B^2\sigma_B^2}{2\pi M}}+\frac{h_{B,m}\sqrt{\xi P}}{2\sqrt{M}}\right)\right]+\sqrt{\frac{h_{B,m}\varsigma_B^2\sigma_B^2}{2\pi M}}+\frac{h_{B,m}\sqrt{\xi P}}{2\sqrt{M}}. \tag{A24}$$

R_3 in (A23) is a function of μ. We need to find a smaller value of R_3 to obtain a tight upper constraint on secrecy capacity. Here, we will look at three scenarios: when $\mu \le 0$, $R_3 \ge \sqrt{\frac{h_{B,m}\varsigma_B^2\sigma_B^2}{2\pi M}}+\frac{h_{B,m}\sqrt{\xi P}}{2\sqrt{M}}$, when $\mu \ge \frac{h_{B,m}}{h_{E,m}}$, $R_3 \ge \frac{h_{B,m}}{h_{E,m}\sqrt{2\pi}}$, and when $0 \le \mu \le \frac{h_{B,m}}{h_{E,m}}$, R_3 is obtained in (A24). If $\frac{1}{\sqrt{2\pi}} \ge \frac{h_{B,m}}{h_{E,m}}\left(\sqrt{\frac{h_{B,m}\varsigma_B^2\sigma_B^2}{2\pi M}}+\frac{h_{B,m}\sqrt{\xi P}}{2\sqrt{M}}\right)$, $R_3 \ge \sqrt{\frac{h_{B,m}\varsigma_B^2\sigma_B^2}{2\pi M}}+\frac{h_{B,m}\sqrt{\xi P}}{2\sqrt{M}}$; otherwise $R_3 \ge \frac{h_{B,m}}{h_{E,m}\sqrt{2\pi}}$.

Substituting R_3 into (A23), we obtain *Theorem 2*.

Appendix C

Proof of Asymptotic Behavior (24):

According to *Theorem 1*, $f_{low}(h_{B,m},\xi,P)$ is a monotonically declining positive function concerning $h_{B,m}$, ξ, and P [47]. When P approaches infinity, we can clearly obtain [40]

$$\begin{cases}\lim\limits_{P\to\infty} f_{low}(h_{B,m},\xi,P)=\ln(h_{B,m})\\ \lim\limits_{P\to\infty}\left[e^{\frac{1}{h_{B,m}\varsigma_B^2\xi P}}\mathbb{E}i\left(-\frac{1}{h_{B,m}\varsigma_B^2\xi P}\right)-e^{\frac{1}{h_{E,m}\varsigma_E^2\xi P}}\mathbb{E}i\left(-\frac{1}{h_{E,m}\varsigma_E^2\xi P}\right)\right]\\ \quad=\frac{h_{E,m}\varsigma_E^2}{h_{B,m}\varsigma_B^2}\end{cases}. \tag{A25}$$

We obtain an asymptotic lower bound by putting (A25) into *Theorem 1* as

$$\lim_{P\to\infty} R_s \ge \frac{1}{2}\ln\left(\frac{e}{2\pi}\right)+\frac{1}{2M}\sum_{m=1}^{M}\ln\left(\frac{h_{B,m}\varsigma_E^2\sigma_E^2}{h_{E,m}\varsigma_B^2\sigma_B^2}\right). \tag{A26}$$

With respect to the asymptotic upper bound, when P approaches infinity, we do not encounter the condition of $\frac{1}{\sqrt{2\pi}} \ge \frac{h_{E,m}}{h_{B,m}}\left(\sqrt{\frac{h_{B,m}\varsigma_B^2\sigma_B^2}{2\pi M}}+\frac{h_{B,m}}{2}\sqrt{\frac{\xi P}{M}}\right)$. The asymptote upper bound can be obtained as

$$\lim_{P\to\infty} R_s \le \frac{1}{2}\ln\left(\frac{4e}{\pi^2}\right)+\frac{1}{2M}\sum_{m=1}^{M}\ln\left(\frac{h_{B,m}\varsigma_E^2\sigma_E^2}{h_{E,m}\varsigma_B^2\sigma_B^2}\right). \tag{A27}$$

Appendix D

Proof of Lower bound (27) in *Theorem 3*:

Corresponding to (A.1), the functional optimization problem is

$$\begin{aligned}\max_{f_X(x)}\mathcal{H}(X) &= -\textstyle\int_0^A f_X(x)\ln[f_X(x)]\mathrm{d}x\\ \text{s.t. } &\textstyle\int_0^A f_X(x)\mathrm{d}x=1\\ &\mathbb{E}(X)=\textstyle\int_0^A x f_X(x)\mathrm{d}x=\xi P.\end{aligned} \tag{A28}$$

By employing the variational method, we can determine the input PDF as [11]

$$f_X(x) = e^{cx+b-1}, \tag{A29}$$

where c and b are free parameters. When $c = 0$, replacing the constraints in (A28) with the expression from (A29) yields [11]

$$f_X(x) = \frac{1}{A},\ x \in [0, A] \tag{A30}$$

In this case, $\mathbb{E}_X(X) = \frac{A}{2} = \xi P$. When $\alpha = 0.5$, we can obtain $\mathcal{H}(X) = \ln(A)$ and $\mathrm{var}(\grave{Y}_{E,m}) = \frac{h_{E,m}^2 A^2}{12} + \frac{A}{2} h_{E,m} \varsigma_E^2 \sigma_E^2 + \sigma_E^2$. Furthermore, $\mathbb{E}_x\left[\ln\left(\frac{1+h_{E,m} X \varsigma_E^2}{1+h_{B,m} X \varsigma_B^2}\right)\right]$ in (13) can be obtained as [40]

$$\mathbb{E}_x\left[\ln\left(\frac{1+h_{E,m} X \varsigma_E^2}{1+h_{B,m} X \varsigma_B^2}\right)\right] = \ln\left(\frac{1+h_{E,m} A \varsigma_E^2}{1+h_{B,m} A \varsigma_B^2}\right) - \frac{\ln(1+h_{B,m} A \varsigma_B^2)}{A - h_{B,m} \varsigma_B^2} + \frac{\ln(1+h_{E,m} A \varsigma_E^2)}{A h_{E,m} \varsigma_E^2}. \tag{A31}$$

Then, we substitute $\mathcal{H}(X)$, $\mathrm{var}(Y_{E,m})$, and (A31) into (13), the lower bound is obtained for $\alpha = 0.5$.

When $c \neq 0$, we have $\alpha \neq 0.5$, Replacing the constraints in (A28) with the expression from (A29) yields [11]

$$f_X(x) = \frac{c e^{cx}}{e^{cA} - 1},\ x \in [0, A] \tag{A32}$$

where c is the solution to (30). Therefore, we obtain $\mathcal{H}(X) = \ln\left(\frac{e^{cA}-1}{c}\right) - c\xi P$. Then, we obtain (A33) and (A34) as

$$\mathrm{var}(Y_{E,m}) = h_{E,m}^2 \left[\frac{A(cA-2)}{c(1-e^{-cA})} + \frac{2}{c^2} - \xi^2 P^2\right] + h_{E,m} \xi P \varsigma_E^2 \sigma_E^2 + \sigma_E^2. \tag{A33}$$

$$\begin{aligned}\mathbb{E}_x\left[\ln\left(\frac{1+h_{E,m} X \varsigma_E^2}{1+h_{B,m} X \varsigma_B^2}\right)\right] = \frac{1}{e^{cA}-1}\Bigg\{&\ln\left(\frac{1+h_{E,m} A \varsigma_E^2}{1+h_{B,m} A \varsigma_B^2}\right) e^{cA} - e^{-\frac{c}{h_{E,m}\varsigma_E^2}}\left[Ei\left(\frac{c\left(1+h_{E,m} A \varsigma_E^2\right)}{h_{E,m}\varsigma_E^2}\right) - \right.\\ &\left. Ei\left(\frac{c}{h_{E,m}\varsigma_E^2}\right)\right] + e^{-\frac{c}{h_{B,m}\varsigma_B^2}} i\left(\frac{c\left(1+h_{B,m} A \varsigma_B^2\right)}{h_{B,m}\varsigma_B^2}\right) - Ei\left(\frac{c}{h_{B,m}\varsigma_B^2}\right)\Bigg\}.\end{aligned} \tag{A34}$$

Substituting $\mathcal{H}(X)$, (A33) and (A34) into (13), the lower bound is obtained for $\alpha \neq 0.5$.

Appendix E

Proof of Upper bound (32) in *Theorem 4*:

In this case, (A5) and (A6) hold; therefore I_1 can be represented as (A11). For I_2, we choose $g_{\grave{Y}_{B,m}|\grave{Y}_{E,m}}$ in (A6) as [40]

$$g_{\grave{Y}_{B,m}|\grave{Y}_{E,m}} = \frac{1}{\sqrt{2\pi s^2}} e^{-\frac{(\grave{y}_{B,m} - \mu \grave{y}_{B,m})^2}{2s^2}}, \tag{A35}$$

where μ and s represent two free parameters. Subsequently, I_2 is written as

$$I_2 = \mathbb{E}_{X^* \grave{Y}_{B,m}}\left\{\frac{1}{2}\ln\left(2\pi s^2\right) + \frac{1}{2s^2}\underbrace{\int_{-\infty}^{\infty} \frac{e^{-\frac{\left(\grave{y}_{E,m} - \frac{h_{E,m}}{h_{B,m}} \grave{Y}_{B,m}\right)^2}{2(MX+N)}}}{\sqrt{2\pi(MX+N)}} \left(\grave{Y}_{B,m} - \mu \grave{y}_{E,m}\right)^2 d\grave{y}_{E,m}}_{R_4}\right\}, \tag{A36}$$

where R_4 can be written as

$$R_4 = \left(1 - \mu \frac{h_{E,m}}{h_{B,m}}\right)^2 \grave{Y}_{B,m}^2 + \mu^2 (MX + N). \tag{A37}$$

Then, we substitute R_4 in (A36); I_2 is written in (A38). The inequality holds because $X \leq A$.

$$I_2 \leq \mathbb{E}_{X^*} \left\{ \underbrace{\frac{1}{2} \ln\left(2\pi s^2\right) + \frac{1}{2s^2} \left[\left(1 - \mu \frac{h_{E,m}}{h_{B,m}}\right)^2 \left(h_{B,m}^2 AX + h_{B,m} X \varsigma_B^2 \sigma_B^2 + \sigma_B^2\right) + \mu^2 (MX + N) \right]}_{R_5} \right\} \tag{A38}$$

Using the first partial derivative of R_5 in (A38) with s^2 and setting it to zero, we can find the minimum point as

$$s^2 = \left(1 - \mu \frac{h_{E,m}}{h_{B,m}}\right)^2 \left(h_{B,m}^2 AX + h_{B,m} X \varsigma_B^2 \sigma_B^2 + \sigma_B^2\right) + \mu^2 (MX + N). \tag{A39}$$

By substituting (A39) into (A38), R_5 can be obtained as

$$R_5 = \frac{1}{2} \ln \left\{ 2\pi e \left[\left(1 - \mu \frac{h_{E,m}}{h_{B,m}}\right)^2 \left(h_{B,m}^2 AX + h_{B,m} X \varsigma_B^2 \sigma_B^2 + \sigma_B^2\right) + \mu^2 (MX + N) \right] \right\}. \tag{A40}$$

Putting (A11), (A38) and (A40) into (A5) and utilizing Jensen's inequality for $\ln(\cdot)$ gives us the upper bound as

$$\begin{aligned} R_s \leq -\tfrac{1}{2M} \textstyle\sum_{m=1}^{M} \Bigg\{ & \ln\left(2\pi e \tfrac{\sigma_B^2}{\sigma_E^2}\right) - \tfrac{1}{2} \ln\left[\mathbb{E}_{X^*} \left(\tfrac{1 + h_{B,m} X \varsigma_B^2}{1 + h_{E,m} X \varsigma_E^2} \right) \right] + \tfrac{1}{2} \ln [2\pi e (1 - \\ & \mu \tfrac{h_{E,m}}{h_{B,m}})^2 \mathbb{E}_{X^*} \left(\tfrac{h_{B,m}^2 AX + h_{B,m} X \varsigma_B^2 \sigma_B^2 + \sigma_B^2}{MX + N} \right) + \mu^2 \right] \Bigg\}. \end{aligned} \tag{A41}$$

We are primarily concerned with the performance at high optical intensities. As A approaches infinity, the input PDF secrecy rate will also reach infinite [47]. Consequently, when A approaches infinity, we obtain

$$\begin{cases} \mathbb{E}_{X^*} \left[\ln\left(\frac{1 + h_{B,m} X \varsigma_B^2}{1 + h_{E,m} X \varsigma_E^2} \right) \right] = \frac{1 + h_{B,m} A \varsigma_B^2}{1 + h_{E,m} A \varsigma_E^2} \\ \mathbb{E}_{X^*} \left[\frac{h_{B,m}^2 AX + h_{B,m} X \varsigma_B^2 \sigma_B^2 + \sigma_B^2}{MX + N} \right] = \frac{h_{B,m}^2 A^2 + h_{B,m} A \varsigma_B^2 \sigma_B^2 + \sigma_B^2}{MX + N}. \end{cases} \tag{A42}$$

Utilizing L'Hospital's rule, we obtain

$$\begin{cases} \lim\limits_{A \to \infty} \frac{1 + h_{B,m} A \varsigma_B^2}{1 + h_{E,m} A \varsigma_E^2} = \frac{h_{B,m} \varsigma_B^2}{h_{E,m} \varsigma_E^2} \\ \lim\limits_{A \to \infty} \frac{h_{B,m}^2 A^2 + h_{B,m} A \varsigma_B^2 \sigma_B^2 + \sigma_B^2}{MX + N} = \frac{h_{B,m}^2 A + h_{B,m} \varsigma_B^2 \sigma_B^2}{M} \end{cases} \tag{A43}$$

In accordance with (A41)–(A43), the upper bound can be asymptotically obtained as

$$R_s \leq -\frac{1}{2M} \sum_{m=1}^{M} \left\{ \ln\left(2\pi e \frac{h_{B,m} \varsigma_B^2 \sigma_B^2}{h_{E,m} \varsigma_E^2 \sigma_E^2}\right) + \frac{1}{2} \ln \left[\underbrace{2\pi e \left(\left(1 - \mu \frac{h_{E,m}}{h_{B,m}}\right)^2 \frac{h_{B,m}^2 A + h_{B,m} \varsigma_B^2 \sigma_B^2}{M} + \mu^2 \right)}_{R_6} \right] \right\}, \tag{A44}$$

Using the first partial derivative of R_6 regarding μ and setting it to 0, (A45) is obtained. Putting (A45) into (A44), we obtain (32).

$$\mu = \frac{\frac{h_{E,m}}{h_{B,m}} \frac{h_{B,m}^2 A + h_{B,m}\varsigma_B^2\sigma_B^2}{M}}{1 + \left(\frac{h_{E,m}}{h_{B,m}}\right)^2 \frac{h_{B,m}^2 A + h_{B,m}\varsigma_B^2\sigma_B^2}{M}}. \tag{A45}$$

Appendix F

Proof of Upper bound (34) in *Corollary 6*:

The ratio of the average to the maximum optical intensity, $\alpha \in (0, 1]$, is a constant that is always positive, and $\alpha A = \xi P$. When A approaches closer and closer to infinity, so does P. When $\alpha = 0.5$, we have [40]

$$\lim_{A\to\infty} f_{low}(h_{B,m}, \xi, P) = \lim_{P\to\infty} f_{low}(h_{B,m}, \xi, P) = \ln(h_{B,m}). \tag{A46}$$

Utilizing L'Hospital's rule, we obtain

$$\begin{cases} \lim\limits_{A\to\infty} \frac{1}{2}\ln\left(\frac{1+h_{E,m}A\varsigma_E^2}{1+h_{B,m}A\varsigma_B^2}\right) = \frac{1}{2}\ln\left(\frac{h_{E,m}\varsigma_E^2}{h_{B,m}\varsigma_B^2}\right) \\ \lim\limits_{A\to\infty} \frac{\ln\left(1+h_{B,m}A\varsigma_B^2\right)}{2Ah_{B,m}\varsigma_B^2} = 0 \\ \lim\limits_{A\to\infty} \frac{\ln\left(1+h_{E,m}A\varsigma_E^2\right)}{2Ah_{E,m}\varsigma_E^2} = 0 \\ \lim\limits_{A\to\infty} \frac{1}{2}\ln\left(\frac{6A^2\sigma_B^2}{\pi e\sigma_B^2\left(h_{E,m}^2A^2h_{E,m}\varsigma_E^2\sigma_E^2+12\sigma_E^2\right)}\right) = \frac{1}{2}\ln\left(\frac{6\sigma_E^2}{\pi e\sigma_B^2 h_{E,m}^2}\right). \end{cases} \tag{A47}$$

Based on (A46) and (A47), the asymptotic lower bound is computed when $\alpha = 0.5$ as

$$\lim_{A\to\infty} R_s \le \frac{1}{2M}\sum_{m=1}^{M} \ln\left(\frac{6h_{B,m}\varsigma_E^2\sigma_E^2}{\pi e h_{E,m}\varsigma_B^2\sigma_B^2}\right). \tag{A48}$$

When $\alpha \neq 0.5$, (A46) can also be obtained. Based on (A34)–(A43), we have

$$\begin{aligned} \lim_{A\to\infty} \frac{1}{2\left(e^{cA}-1\right)} \Bigg\{ \ln\left(\frac{1+h_{E,m}A\varsigma_E^2}{1+h_{B,m}A\varsigma_B^2}\right) e^{cA} - e^{-\frac{c}{h_{E,m}\varsigma_E^2}} \left[Ei\left(\frac{c\left(1+h_{E,m}A\varsigma_E^2\right)}{h_{E,m}\varsigma_E^2}\right) - Ei\left(\frac{c}{h_{E,m}\varsigma_E^2}\right)\right] + \\ e^{-\frac{c}{h_{B,m}\varsigma_B^2}} i\left(\frac{c\left(1+h_{B,m}A\varsigma_B^2\right)}{h_{B,m}\varsigma_B^2}\right) - Ei\left(\frac{c}{h_{B,m}\varsigma_B^2}\right)\Bigg\} = \frac{1}{2}\ln\left(\frac{h_{E,m}\varsigma_E^2}{h_{B,m}\varsigma_B^2}\right). \end{aligned} \tag{A49}$$

Thus, we attain the asymptotic lower bound when $\alpha \neq 0.5$ as

$$\lim_{A\to\infty} R_s \frac{1}{2M}\sum_{m=1}^{M} \ln\left[\frac{h_{B,m}h_{E,m}\varsigma_E^2\sigma_E^2\left(e^{cA}-1\right)^2}{2\pi e c^2\varsigma_B^2\sigma_B^2 e^{2e\xi P}\left[h_{E,m}^2\left(\frac{A(cA-2)}{c\left(1-e^{-cA}\right)} + \frac{2}{c^2} - \xi^2P^2\right) + h_{E,m}\xi P\varsigma_E^2\sigma_E^2 + \sigma_E^2\right]}\right]. \tag{A50}$$

We obtain the asymptotic upper bound as

$$\lim_{A\to\infty} R_s \le \frac{1}{2M}\sum_{m=1}^{M} \ln\left(\frac{h_{B,m}\varsigma_E^2\sigma_E^2}{h_{E,m}\varsigma_B^2\sigma_B^2}\right). \tag{A51}$$

Based on (A48), (A50) and (A51), *Corollary 6* is verified.

References

1. Matthaiou, M.; Yurduseven, O.; Ngo, H.Q.; Morales-Jimenez, D.; Cotton, S.L.; Fusco, V.F. The Road to 6G: Ten Physical Layer Challenges for Communications Engineers. *IEEE Commun. Mag.* **2021**, *59*, 64–69. [CrossRef]
2. Ishikawa, N.; Sugiura, S.; Hanzo, L. 50 Years of Permutation, Spatial and Index Modulation: From Classic RF to Visible Light Communications and Data Storage. *IEEE Commun. Surv. Tutor.* **2018**, *20*, 1905–1938. [CrossRef]

3. Di Renzo, M.; Haas, H.; Ghrayeb, A.; Sugiura, S.; Hanzo, L. Spatial Modulation for Generalized MIMO: Challenges, Opportunities, and Implementation. *Proc. IEEE* **2014**, *102*, 56–103. [CrossRef]
4. Yang, P.; Di Renzo, M.; Xiao, Y.; Li, S.; Hanzo, L. Design Guidelines for Spatial Modulation. *IEEE Commun. Surv. Tutor.* **2014**, *17*, 6–25. [CrossRef]
5. Wen, M.; Zheng, B.; Kim, K.J.; Di Renzo, M.; Tsiftsis, T.A.; Chen, K.-C.; Al-Dhahir, N. A Survey on Spatial Modulation in Emerging Wireless Systems: Research Progresses and Applications. *IEEE J. Sel. Areas Commun.* **2019**, *37*, 1949–1972. [CrossRef]
6. Li, J.; Dang, S.; Wen, M.; Li, Q.; Chen, Y.; Huang, Y.; Shang, W. Index Modulation Multiple Access for 6G Communications: Principles, Applications, and Challenges. *IEEE Netw.* **2023**, *37*, 52–60. [CrossRef]
7. Al-Moliki, Y.M.; Alresheedi, M.T.; Abas, A.F.; Mahdi, M.A.; Khoon, N.E. OFDM-Based Time-Domain Optical MIMO with General-Numbered LED Configurations. *Opt. Quantum Electron.* **2023**, *55*, 1093. [CrossRef]
8. Rohner, S.; Raza, D.; Puccinelli, D.; Voigt, T. Security in Visible Light Communication: Novel Challenges and Opportunities. *Sens. Transducers* **2015**, *192*, 9–15.
9. Blinowski, G. Security Issues in Visible Light Communication Systems. In Proceedings of the 13th IFAC and IEEE Conference on Programming Devices and Embedded Systems, Cracow, Poland, 13–15 May 2015; Elsevier Science Direct: Amsterdam, The Netherlands, 2015; Volume 48, pp. 234–239.
10. Hamamreh, J.M.; Furqan, H.M.; Arslan, H. Classifications and Applications of Physical Layer Security Techniques for Confidentiality: A Comprehensive Survey. *IEEE Commun. Surveys Tutor.* **2019**, *21*, 1773–1828. [CrossRef]
11. Wang, J.; Liu, C.; Wang, J.; Wu, Y.; Lin, M.; Cheng, J. Physical-Layer Security for Indoor Visible Light Communications: Secrecy Capacity Analysis. *IEEE Trans. Commun.* **2018**, *66*, 6423–6436. [CrossRef]
12. Che, Z.; Fang, J.; Jiang, Z.L.; Li, J.; Zhao, S.; Zhong, Y.; Chen, Z. A Physical-Layer Secure Coding Scheme for Indoor Visible Light Communication Based on Polar Codes. *IEEE Photon. J.* **2018**, *10*, 7907313. [CrossRef]
13. Chen, J.; Shu, T. Statistical Modeling and Analysis on the Confidentiality of Indoor VLC Systems. *IEEE Trans. Wirel. Commun.* **2020**, *19*, 4744–4757. [CrossRef]
14. Kumar, P.; Garg, A.; Gupta, A. PLS Analysis in an Indoor Heterogeneous VLC/RF Network Based on Known and Unknown CSI. *IEEE Syst. J.* **2021**, *15*, 68–76. [CrossRef]
15. Pham, T.V.; Pham, A.T. On the Secrecy Sum-Rate of MU-VLC Broadcast Systems with Confidential Messages. In Proceedings of the 10th International Symposium on Communication Systems, Networks and Digital Signal Processing (CSNDSP), Prague, Czech Republic, 20–22 July 2016; IEEE: New York, NY, USA, 2016; pp. 1–6.
16. Yin, L.; Haas, H. Physical-Layer Security in Multiuser Visible Light Communication Networks. *IEEE J. Sel. Areas Commun.* **2018**, *36*, 162–174. [CrossRef]
17. Zhao, X.; Chen, H.; Sun, J. On Physical-Layer Security in Multiuser Visible Light Communication Systems with Non-Orthogonal Multiple Access. *IEEE Access* **2018**, *6*, 34004–34017. [CrossRef]
18. Su, N.; Panayirci, E.; Koca, M.; Yesilkaya, A.; Poor, H.V.; Haas, H. Physical Layer Security for Multi-User MIMO Visible Light Communication Systems with Generalized Space Shift Keying. *IEEE Trans. Commun.* **2021**, *69*, 2585–2598. [CrossRef]
19. Pan, G.; Ye, J.; Ding, Z. On Secure VLC Systems With Spatially Random Terminals. *IEEE Commun. Lett.* **2017**, *21*, 492–495. [CrossRef]
20. Ma, S.; Dong, Z.-L.; Li, H.; Lu, Z.; Li, S. Optimal and Robust Secure Beamformer for Indoor MISO Visible Light Communication. *J. Light. Technol.* **2016**, *34*, 4988–4998. [CrossRef]
21. Mostafa, A.; Lampe, L. Optimal and Robust Beamforming for Secure Transmission in MISO Visible-Light Communication Links. *IEEE Trans. Signal Process.* **2016**, *64*, 6501–6516. [CrossRef]
22. Arfaoui, M.A.; Rezki, Z.; Ghrayeb, A.; Alouini, M.S. On the Input Distribution and Optimal Beamforming for the MISO VLC Wiretap Channel. In Proceedings of the IEEE Global Conference on Signal and Information Processing (GlobalSIP), Washington, DC, USA, 7–9 December 2016; IEEE: New York, NY, USA, 2016; pp. 970–974.
23. Arfaoui, M.A.; Rezki, Z.; Ghrayeb, A.; Alouini, M.S. On the Secrecy Capacity of MISO Visible Light Communication Channels. In Proceedings of the IEEE Global Communications Conference (GLOBECOM), Washington, DC, USA, 4–8 December 2016; IEEE: New York, NY, USA; pp. 1–7.
24. Mostafa, A.; Lampe, L. Physical-Layer Security for MISO Visible Light Communication Channels. *IEEE J. Sel. Areas Commun.* **2015**, *33*, 1806–1818. [CrossRef]
25. Wang, J.-Y.; Yu, Y.-C.; Lu, D.-S.; Su, D.-P. Secure Beamforming for MISO Visible Light Communications with ISI and NLoS Components. *IEEE Wirel. Commun. Lett.* **2024**, *13*, 908–912. [CrossRef]
26. Mostafa, A.; Lampe, L. Securing Visible Light Communications via Friendly Jamming. In Proceedings of the IEEE Globecom Workshops (GC Wkshps), Austin, TX, USA, 8–12 December 2014; IEEE: New York, NY, USA; pp. 524–529.
27. Zaid, H.; Rezki, Z.; Chaaban, A.; Alouini, M.S. Improved Achievable Secrecy Rate of Visible Light Communication with Cooperative Jamming. In Proceedings of the IEEE Global Conference on Signal and Information Processing (GlobalSIP), Orlando, FL, USA, 4–16 December 2015; IEEE: New York, NY, USA; pp. 1165–1169.
28. Pham, T.V.; Hayashi, T.; Pham, A.T. Artificial-Noise-Aided Precoding Design for Multi-User Visible Light Communication Channels. *IEEE Access* **2019**, *7*, 3767–3777. [CrossRef]
29. Pham, T.V.; Pham, A.T. Energy Efficient Artificial Noise-Aided Precoding Designs for Secured Visible Light Communication Systems. *IEEE Trans. Wirel. Commun.* **2021**, *20*, 653–666. [CrossRef]

30. Wang, J.-Y.; Hong, L.-H.; Liu, N.; Yang, H.-N.; Feng, P.; Ren, J. Secrecy Analysis and Optimization for IRMA- and Jammer-Aided Visible Light Communications. *IEEE Wirel. Commun. Lett.* **2024**, *13*, 1908–1912. [CrossRef]
31. Pham, T.V.; Pham, A.T.; Ishihara, S. Design of Energy-Efficient Artificial Noise for Physical Layer Security in Visible Light Communications. *IEEE Trans. Green Commun. Netw.* **2024**, *8*, 741–755. [CrossRef]
32. Shen, H.; Deng, Y.; Xu, W.; Zhao, C. Secrecy-Oriented Transmitter Optimization for Visible Light Communication Systems. *IEEE Photon. J.* **2016**, *8*, 7905914. [CrossRef]
33. Cho, S.; Chen, G.; Coon, J.P. Enhancement of Physical Layer Security with Simultaneous Beamforming and Jamming for Visible Light Communication Systems. *IEEE Trans. Inf. Forensics Secur.* **2019**, *14*, 2633–2648. [CrossRef]
34. Mukherjee, P. Secret-Key Agreement for Security in Multi-Emitter Visible Light Communication Systems. *IEEE Commun. Lett.* **2016**, *20*, 1361–1364. [CrossRef]
35. Al-Moliki, Y.M.; Alresheedi, M.T.; Al-Harthi, Y. Improving Availability and Confidentiality via Hyperchaotic Baseband Frequency Hopping Based on Optical OFDM in VLC Networks. *IEEE Access* **2020**, *8*, 125013–125028. [CrossRef]
36. Al-Moliki, Y.M.; Alresheedi, M.T.; Al-Harthi, Y. Design of Physical Layer Key Generation Encryption Method Using ACO-OFDM in VLC Networks. *IEICE Trans. Commun.* **2020**, *E103.B*, 969–978. [CrossRef]
37. Al-Moliki, Y.M.; Alresheedi, M.T.; Al-Harthi, Y.; Alqahtani, A.H. Robust Lightweight Channel-Independent OFDM-Based Encryption Method for VLC-IoT Networks. *IEEE Internet Things J.* **2022**, *9*, 4661–4676. [CrossRef]
38. Alresheedi, M.T.; Al-Moliki, Y.M.; Al-Harthi, Y.; Alqahtani, A.H. Dynamic Hyperchaotic Key Generation Using Optical Orthogonal Frequency Division Multiplexing-Based Visible Light Communication Networks. *IEEJ Trans. Elec. Electron. Eng.* **2022**, *17*, 695–704. [CrossRef]
39. Soltani, M.; Rezki, Z. Optical Wiretap Channel with Input-Dependent Gaussian Noise under Peak-and Average-Intensity Constraints. *IEEE Trans. Inf. Theory* **2018**, *64*, 6878–6893. [CrossRef]
40. Wang, J.-Y.; Yu, P.F.; Fu, X.T.; Wang, J.B.; Lin, M.; Cheng, J.; Alouini, M.S. Secrecy-Capacity Bounds for Visible Light Communications with Signal-Dependent Noise. *IEEE Trans. Wirel. Commun.* **2023**, *22*, 7227–7242. [CrossRef]
41. Li, H.; Wang, F.; Zhang, J.; Liu, C. Secrecy Performance Analysis of MISO Visible Light Communication Systems with Spatial Modulation. *Digit. Signal Process.* **2018**, *81*, 116–128. [CrossRef]
42. Wang, F.; Li, R.; Zhang, J.; Shi, S.; Liu, C. Enhancing the Secrecy Performance of the Spatial Modulation Aided VLC Systems with Optical Jamming. *Signal Process.* **2019**, *157*, 288–302. [CrossRef]
43. Ge, H.; Dai, J.; Huang, B.; Wang, J. Secrecy Rate Analysis for Visible Light Communications Using Spatial Modulation. In Proceedings of the IEEE 21st International Conference on High Performance Computing and Communications (HPCC), Zhangjiajie, China, 10–12 August 2019; IEEE: New York, NY, USA, 2019; pp. 1241–1248.
44. Wang, J.-Y.; Ge, H.; Lin, M.; Wang, J.-B.; Dai, J.; Alouini, M.-S. On the Secrecy Rate of Spatial Modulation-Based Indoor Visible Light Communications. *IEEE J. Sel. Areas Commun.* **2019**, *37*, 2087–2101. [CrossRef]
45. Al-Moliki, Y.M.; Alresheedi, M.T.; Al-Harthi, Y.; Alqahtani, A.H. Channel-Independent Quantum Mapping-Substitution OFDM-Based Spatial Modulation for Physical-Layer Encryption in VLC Networks. *Veh. Commun.* **2024**, *45*, 100706. [CrossRef]
46. Cover, T.; Thomas, J. *Elements of Information Theory*, 2nd ed.; Wiley: Hoboken, NJ, USA, 2006.
47. Moser, S.M. Capacity Results of an Optical Intensity Channel with Input-Dependent Gaussian Noise. *IEEE Trans. Inf. Theory* **2012**, *58*, 207–223. [CrossRef]